AALBORG UNIVERSITET

Department of Energy Technology, Aalborg University, Denmark

Modular Multi-Level Converter: Modeling, Simulation and Control in Steady State and Dynamic Conditions

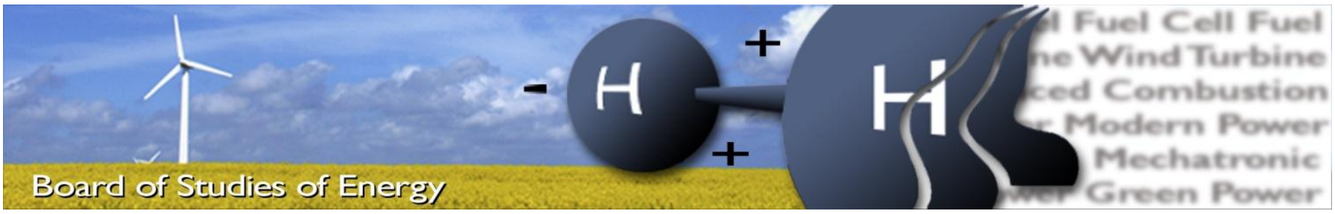

Title: **Modular Multi-Level Converter: Modeling, Simulation and Control in Steady State and Dynamic Conditions**
Semester: **WPS2 (10th)**
Semester theme: **[]**
Project period: **01/02/12 to 30/05/12**
ECTS: **30**
Supervisor: **Remus Teodorescu**
Luca Zarri

SYNOPSIS:

The aim of this project is the analysis of a Modular Multilevel Converter (MMC) and the development of a control scheme for energy stored. The analysis is based on the use of a simplified circuit constituted by a single leg of the converter where all the modules in each arm are represented by a single variable voltage source. Control scheme are thus investigated, focusing on the balancing between upper and lower arm voltage and on the control of the overall energy stored in converter leg.

Project group: **[WPS2 1056]**

____

[Name 1]

Copies: **[2]**
Pages, total: **[83]**
Appendix: **[]**
Supplements: **[]**

By signing this document, each member of the group confirms that all group members have participated in the project work, and thereby all members are collectively liable for the contents of the report. Furthermore, all group members confirm that the report does not include plagiarism.

Preface

This work, carried out by Giacomo Casadei, is a part of the final thesis to accomplish the Master Degree in Automation Engineering at the University of Bologna (Italy). It started at the beginning of February 2012 at the Department of Energy Technology, Aalborg University, and will be completed in Winter 2012 at the University of Bologna, Department of Electrical Engineering.

Prof. Remus Teodorescu, and Prof. Luca Zarri are the supervisors of this thesis.

Aalborg, June 8, 2012

Acknowledgements

I would like to thank my supervisor Prof. Remus Teodorescu for giving me the opportunity to be involved with such a subject that is interesting and modern. I also would like to thank Prof. Luca Zarri for its valuable help and guidance during my study in Automation Engineering. Their advices and comments not only helped me for specific issues but also improved my knowledge.

Additionally the author would like to thank all colleagues met in AAU, with whom he shared this wonderful experience and work, and all his "home" and Danish friends.

Last but not the least, the author would like to thank all his family for infinite support and love."I'll never be able to give you back what you gave me".

A special thanks goes to Earth and Pillars.
Dedicated to silence.

Aalborg, June 8, 2012

Summary

The aim of this project is the analysis of a Modular Multilevel Converter (MMC) and the development of a control scheme for energy stored. The converter is characterized by a modular arm structure, formed by a cascade connection of a large number of simple chopper cells with floating DC capacitors: these cells are called Sub-Modules (SM) and can be easily assembled into a converter for high- or medium-voltage power conversion systems. The analysis is based on the use of a simplified circuit constituted by a single leg of the converter, where all the modules in each arm are represented by a single variable voltage source. The circuit model is derived as a system of differential equations that can be used for analyzing both the steady state and dynamic behavior of the MMC, from voltages and thus energy point of view. The converter structure requires an arm voltage balancing control and a leg total voltage control in order to achieve a stable behavior in all operating conditions. The validity and the effectiveness of the voltage control strategy are confirmed by numerical simulations.

Thesis objective is to deepen control issues about MMC family of converters: in order to approach properly control system, a state of the art analysis had to be done.

This analysis showed that, as of today, few modeling approaches have been investigated and thus, control issues are still difficult to be solved. In fact, it became clear that a different modeling approach will be necessary in order to solve all dynamic operation requirements.

Following a reliable modeling approach, carried out by A. Antonopoulos, L.Angquist, and H.P. Nee in "On dynamics and voltage control of the modular multilevel converter" (European Power Electronics Conference (EPE), Barcelona, Spain, September 8-10, 2009), dynamic behavior of converter voltages and energy has been analyzed.

New and improved regulators have been implemented: in fact, in order to solve dynamic transients of the MMC (for instance LVRT, Failure Mode condition etc.) it became clear that conventional control structures are not sufficient.

The over mentioned modeling approach leads to a highly non-linear system: non-linearity is present also in the input, thus advanced control approach are difficult to be implemented.

Thus, in the fifth chapter of this thesis, a new modeling approach is proposed, aiming to simplify advanced control implementation.

It can be concluded, that with the new modeling approach a significant contribution to control issues will be possible.

Thesis Layout

Chapter I

1. Introduction and Motivations
    1.1. Objectives
    1.2. Limitations

Chapter II

1. Description and Operation Principle of MMC

Chapter III

1. Mathematical Model of the MMC

2. Control Strategy

3. Consideration About Control Strategy And Model

Chapter IV

1. Development of a MATLAB model

2. First Model: Converter Operation and Model Verification

3. Second Model: Energy Control:
    3.1. Simulation Results

4. Third Model: Output Power Control:
    4.1. Simulation Results

5. Fourth Model: Mega-Watt System
    5.1. Capacitance Relationship with Voltage Ripple
    5.2. Simulation Results
    5.3. Simulation Results: Sub-Modules Failure Mode
    5.4. Simulation Results: LVRT

Chapter V

1. Motivations for a New Modeling Approach
2. Modeling Principles and Equations
3. Control Proposal
4. Future Works

Chapter VI - Conclusions

List of symbols – First Model

C : sub-modules capacitor

N : number of sub-modules in each arm

C^{arm}: total capacitance of the arm

C^{m}: equivalent capacitance of the arm *m*

L, R : arm impedance

$n(t)$: general modulation index

u_C^m: *m* arm voltage

$u_C^{\Sigma}(t)$: voltage stored in arm capacitor

$i(t)$: current flowing through the arm

i_U, i_L : upper and lower arm currents respectively

i_V : output current

i_{diff} : differential current

$u_{CU}^{\Sigma}, u_{CL}^{\Sigma}$: upper and lower sub-modules voltages respectively

n_U, n_L : upper and lower modulation indexes respectively

u_D : DC voltage

u_V : output voltage

$m(t), \widehat{m}$: modulation carrier, with $\widehat{m}$ as pick value

u_{CU}, u_{CL} : upper and lower arm voltages respectively

u_{diff} : differential voltage

e_v : internal alternating voltage

$W_{CU}^{\Sigma}, W_{CL}^{\Sigma}$: total energy stored in upper and lower sub-modules respectively

$W_C^{\Sigma}, W_C^{\Delta}$: total energy stored in one phase and difference between upper and lower energy

u_g : grid voltage

L_g, R_g : line impedance

List of symbols – Second Model

V_P, V_N : upper and lower arm voltages respectively

V_O : output voltage

L_P, R_P : upper arm impedance

L_N, R_N : lower arm impedance

i_P, i_N : upper and lower arm currents respectively

i_O : output current

E_{DC} : DC voltage

S_P, S_N : upper and lower modulation indexes respectively

E_P, E_N : upper and lower arm capacitor voltages

C_P, C_N : upper and lower arm equivalent capacitor

$i_{P\,ref}, i_{N\,ref}$: upper and lower arm reference currents

$i_{O\,ref}$: output current reference

$i_{D\,ref}$: differential current reference

$S_{P\,ref}, S_{N\,ref}$: upper and lower modulation indexes reference respectively

$V_{P\,ref}, V_{N\,ref}$: upper and lower arm voltages reference respectively

W_T, W_D: total energy stored in the arm and difference between upper and lower arm energy

$W_{T\,ref}, W_{D\,ref}$: total energy and difference of upper and lower arm energy references

Chapter I

1 – Introduction and Motivations

The development of new technologies and devices during the 20th century enhanced the interest in electric power systems. Modern civilization based his operation on an increasing energy demand and on the substitutions of human activities with complex and sophisticated machines; thus, studies on electric power generation and conversion devices become every day more and more important.

The recent attention in environment protection and preservation increased the interest in electrical power generation from renewable sources: wind power systems and solar systems are diffusing and are supposed to occupy an increasingly important role in world-wide energy production in coming years.

Not only house utilities, but industrial applications and even the electrical network requirements display the importance that energy supply and control will have in the future researches.

As a consequence, power conversion and secondly control is required to be reliable, safe and available in order to accomplish all requirements, both from users and legal regulations, and to reduce the environmental impact.

Voltage Source Converter (VSC) technology is becoming common in high-voltage direct current (HVDC) transmission systems (especially transmission of offshore wind power, among others). HVDC transmission technology is an important and efficient possibility to transmit high powers over long distances.

The vast majority of electric power transmissions were three-phase and this was the common technology widespread. Main advantages for choosing HVDC instead of AC to transmit power can be numerous but still in discussion, and each individual situation must be considered apart. Each project will display its own pro and con about HVDC transmission, but commonly these advantages can be summarized: lower losses, long distance water crossing, controllability, limitation short circuit currents, environmental reason and lower cost.

One of the most important advantages of HVDC on AC systems is related with the possibility to accurately control the active power transmitted, in contrast AC lines power flow can't be controlled in the same direct way.

However conventional converters display problems into accomplishing requirements and operation of HVDC transmission. Compared to conventional VSC technology, Modular Multilevel topology instead offers advantages such as higher voltage levels, modular construction, longer maintenance intervals and improved reliability.

Figure 1 - ABB DolWin Installation, using HVDC connection

A multilevel approach guarantees a reduction of output harmonics due to sinusoidal output voltages: thus grid filters become negligible, leading to system cost and complexity reduction.

Like in many other engineering fields, modular and distributed systems are becoming the suggested topology to achieve modern projects requirements: this configuration ensure a more reliable operation, facilitates diagnosis, maintenance and reconfigurations of control system. Especially in fail safe situations, modular configuration allows control system to isolate the problem, drive the process in safe state easily, and in many cases allows one to reach an almost normal operation even if in faulty conditions.

However, it is necessary to take into account also disadvantages brought by Modular design: the control scheme actually results more complex and requires a “two level” configuration. Each modular part as to be controlled independently, but a master control layer is needed to reach the overall system behaviour requirements. It is necessary to provide a proper division of tasks between local controllers and master controller: must of all, the communication system becomes really important in order to achieve overall stability and time deadline accomplishment.

In the case of MMC, the concept of a modular converter topology has the intrinsic capability to improve the reliability, as a fault module can be bypassed allowing the operation of the whole circuit without affecting significantly the performance.

Many multi-level converter topologies have been investigated in these last years [1], having advantages and disadvantages during operation or when assembling the converters. To solve the problems of conventional multi-level converter a new MMC

topology was proposed in [2]-[5], describing the operation principle and performance under different operating conditions. A simple schematic of this converter with N modules per arm is shown in Fig. 1. The MMC proposed in [2]-[5] is one of the most promising power converter topology for high power applications in the near future, particularly in HVDC links (e.g. transmission of offshore wind power, among others).
Siemens has a plan of putting this converter into practical applications with the trade name "HVDC-plus". The system configuration of the HVDC-plus has a power of 400 MVA, a dc link voltage of 200 kV, and each arm composed of 200 cascaded chopper cells [6].
This converter topology has been investigated by several research teams lately [7]-[12]. These papers where mainly focused on the analysis of simplified circuit models and improved control systems to achieve a reliable and stable operation of the converter, as the cascaded connection of multiple sub-modules in each arm and leg requires the voltage balance among the several sub-modules of each arm and between upper and lower arms. The control of the total leg voltage and differential voltage between upper and lower arms is a crucial point as it can affect seriously the operation of MMC if not properly implemented. The potential interaction between these two loops of control will be deepened and discussed; it will be important to evaluate the possibility of control task distribution; this analysis is required to design the most suitable control scheme.
The aim of this paper is to accomplish the stable voltage control of the MMC in all operating conditions and the theoretical analysis is based on the circuit model proposed in [8], hence, the same terminology will be used. The approach is based on using a continuous model, where all modules in each arm are represented by variable voltage sources, and PWM effects are neglected. The numerical simulations of the converter show the presence of high currents that can circulate through the phase legs, leading to the need of over-rating the modules. Besides to this, the presence of these currents produces an energy transfer between the arms, leading to possible instabilities of the converter. A suitable control strategy has been implemented for avoiding instabilities in all operating conditions. The validity and the effectiveness of the voltage control strategy is confirmed by numerical simulations.

1.1 – Objectives

In this thesis, analysis, modeling and control of a 13 MW/20 KV MMC converter are investigated. Thus, objectives can be summarized:

- MMC operation principles: state of art and actual achievement
- MMC modeling: analysis of modeling approaches available
- Modeling Development and Simulation Verification of a KW system

- Modeling Development and Simulation Verification of a MW system
- Control Strategies Analysis and Implementation: firstly on the KW system, then applied and verified on the MW system
- New proposal for modeling and control

1.2 – Limitations

This thesis main objective is to find a performing control system for the energy stored in the converter: even if MMC is a well-known topology of converter, few modeling and control approach are available.
To carry out this primary analysis, a modeling approach has been chosen and followed, and can be found in [8]: this approach showed to be the most promising, both for the analysis of MMC operation and for the development of control structure.
However, in Chapter V of this thesis a new modeling approach is suggested, in order to simplify control strategy study.
Being the energy monitoring and control the aim of this project, modeling neglects low level operation and dynamics of the system: sub-modules are simplified with an equivalent variable voltage source, ideally controlled.
This assumption, gives the opportunity to study the system from a proper point of view in terms of energy: on the other side, sub-modules operation is hidden and all issues connected are not dealt in this thesis.
A different approach should be investigated, in order to account also sub-modules operation in the modeling and through this, in control strategy development.

Chapter II

1- Description and principle of operation of MMC

The typical structure of a MMC is shown in Fig. 2, and the configuration of a Sub-Module (SM) is given in Fig. 3. Each SM is a simple chopper cell composed of two IGBT switches (*T1* and *T2*), two anti-parallel diodes (*D1* and *D2*) and a capacitor *C*. Each phase leg of the converter has two arms, each one constituted by a number N of SMs. In each arm there is also a small inductor to compensate for the voltage difference between upper and lower arms produced when a SM is switched in or out.

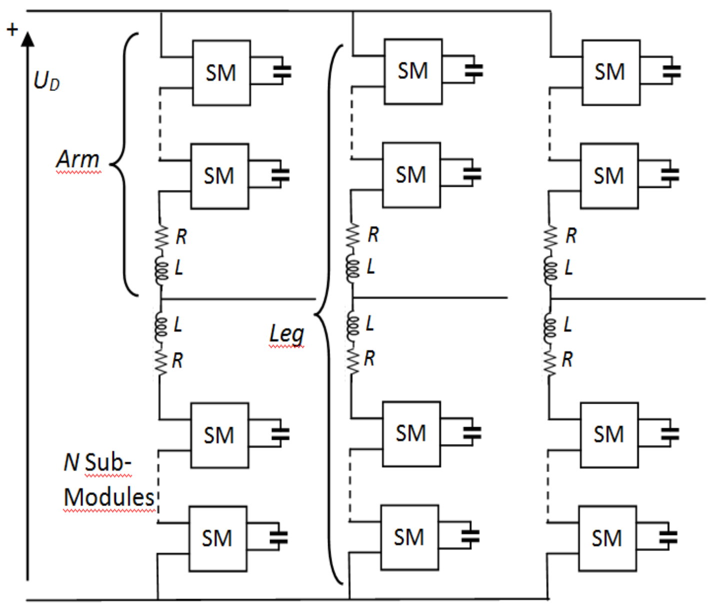

Figure 2 - Schematic of a three-phase Modular Multi-level Converter

With reference to the SM shown in Fig. 2, the output voltage U_O is given by,

$U_O = U_C$ if *T1* is *ON* and *T2* is *OFF*

$U_O = 0$ if *T1* is *OFF* and *T2* is *ON*

where U_C is the instantaneous capacitor voltage.

The configuration with T_1 and T_2 both *ON* should not be considered because it determines a short circuit across the capacitor. Also the configuration with T_1 and T_2 both *OFF* is not useful as it produces different output voltages depending on the current direction. Fig. 4 shows the current flows in both useful states.

In a MMC the number of steps of the output voltage is related to the number of series connected SMs. In order to show how the voltage levels are generated, in the following, reference is made to the simple three level MMC configuration shown in Fig. 5.

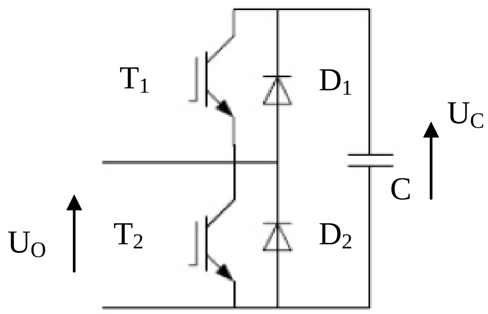

Figure 3 – Chopper cell of a Sub-Module

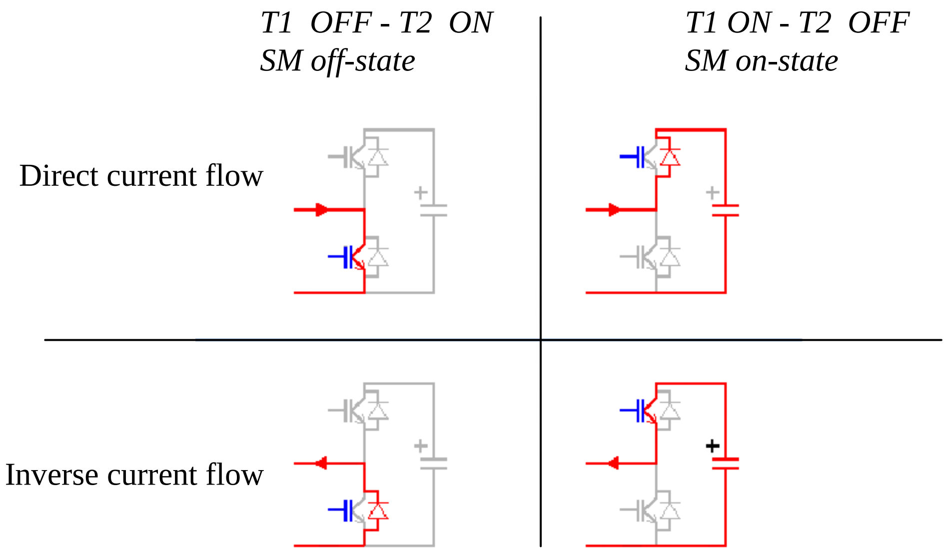

Figure 4 - States of SM and current paths

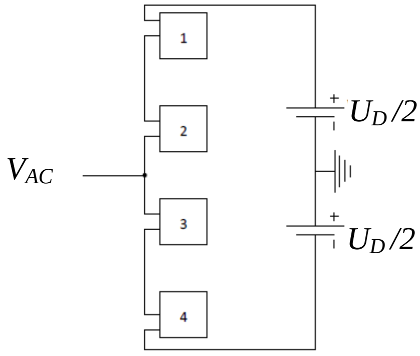

Figure 5 - Schematic of one phase of Three-Level Converter

In this case, in order to get the positive output, $+U_D/2$, the two upper SMs 1 and 2 are bypassed. Accordingly, for the negative output, - $U_D/2$, the two lower SMs 3 and 4 are bypassed. The zero state can be obtained through two possible switch configurations. The first one is when the two SMs in the middle of a leg (2 and 3) are bypassed, and the second one is when the end SMs of a leg (1 and 4) are bypassed. It has to be noted that the current flows through the SM_S that are not by passed determining the charging or discharging of the capacitors depending on the current direction. Therefore, in order to keep the capacitor voltages balanced, both zero states must be used alternatively. The voltage waveform generated by the three level converters is shown in Fig. 6.

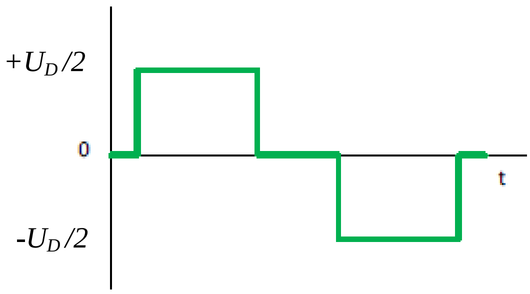

Figure 6 - Voltage waveform of a Three-Level Converter

The principle of operation can be extended to any multi-level configuration as the one represented in Fig. 7.

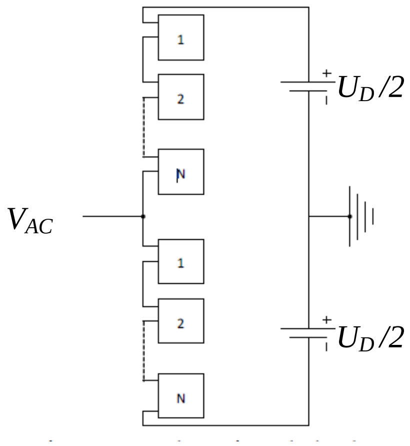

Figure 7 - Schematic of one phase of Multi-Level Converter

In this type of inverter, the only states that have no redundant configurations are the two states that generate the maximum positive and negative voltages, + $U_D/2$ and $–U_D/2$. For generating the other levels, in general there are several possible switching configurations that can be selected in order to keep the capacitor voltages balanced. In MMC of Fig. 6, the switching sequence is controlled so that at each instant only N SMs (i.e. half of the 2N SMs of a phase leg) are in the on-state. As an example, if at a given instant in the upper arm SMs from 2 to N are in the on-state, in the lower arm only one SM will be in on-state. It is clear that there are several possible switching configurations. Equal voltage sharing among the capacitor of each arm can be achieved by a selection algorithm of inserted or bypassed SMs during each sampling period of the control system. A typical voltage waveform of a multi-level converter is shown in Fig. 8.

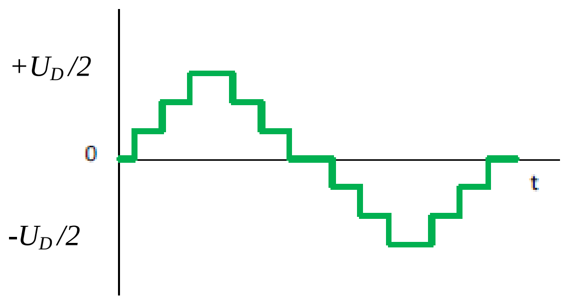

Figure 8 - Voltage waveform of a Multi-Level Converter

Chapter III

3.1 - Mathematical model of the MMC

The typical structure of an MMC, shown in Fig. 1, can be summarized into 3 levels:

I. sub-modules SM (the lower level, usually Chopper cells)
II. arm (second level of the converter, half of the leg-phase)
III. leg (can be considered one phase)

If a two-level control structure is considered, for instance a Master-Slave structure, lower level of control is assigned to sub-models (level I), instead upper level of control deals with arm-leg voltage and currents control (level II, III). It is assumed that a lower level control for the sub-modules is present ensuring that all capacitors are equally charged.
As suggested in [13], most of existing investigations and simulations are based on switched or discrete models. However, discrete models have two main disadvantages:

a) discrete models do not allow an analytical approach to model the converter and to design the control system;
b) numerical solution of complex converter configurations using a high number of SMs require considerable simulation time.

A continuous model can overcome these disadvantages. Therefore, to clearly understand the operation of this converter it is necessary to write the voltage-current equations and to determine a continuous model suitable to design a control scheme.
In the following, an analysis is carried out with the aim to control the upper and lower arm voltages, using the continuous model presented in [8], that considers only one converter phase and is based on time-variable capacitors.
Considering a converter with N sub-modules per arm, each arm can be controlled with an insertion index (modulation index) $n(t)$, where $n(t)=0$ means that all sub-modules in the arm are by-passed, on the other side $n(t)=1$ means that all the sub-modules in the arm are inserted.
Ideal capacitance of the arm should be:

$$C^{arm} = \frac{C}{N} \tag{1}$$

The effective capacitance of the arm is dependent on the insertion index, so it can be written as:

$$C^m = \frac{C^{arm}}{n(t)} \tag{2}$$

where the *m* apex means the number of the arm (for instance, in a three-phase converter *m=1,2,3,..,6*).
It would be possible to have a full representation of the MMC converter, including operation of each sub-module, but this approach tends to be fairly complicated and not easy to be used as a base for control schemes development.
A simpler way would be to consider a continuous model, but 2 important assumptions are necessary in order to develop this approach:

1. the switching frequency is much higher than the frequency of the output voltage
2. the resolution of the output voltage is small, compared to the amplitude of the output voltage (i.e. high number of sub-modules)

Assuming 1 and 2, it's possible to create a continuous model which represents the overall operation of the converter, neglecting the single sub-modules behaviour: this type of model is suitable for control system design and makes it possible to focus on the energy stored in the converter and its balance between arms. The simplified model is shown in Fig. 9.

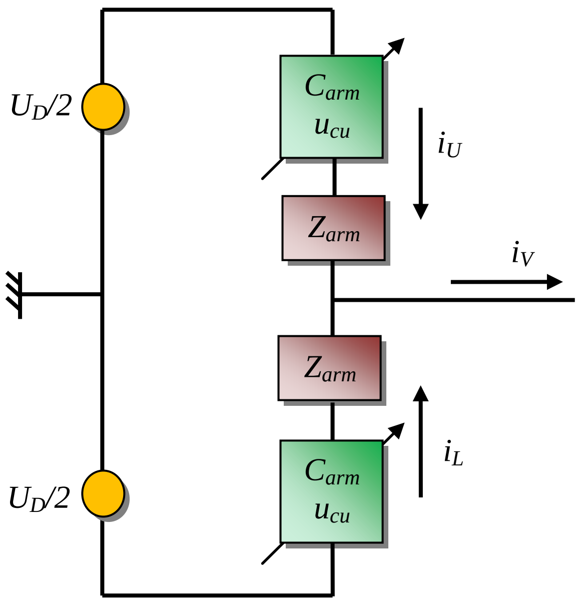

Figure 9 - Simplified Circuit Used for the Analysis

Again, apex *m* represent the arm, *n(t)* is the insertion index, instead $u_c^{\Sigma}(t)$ is the sum of all capacitance voltage in the *m* arm. Then equations (3) and (4) follow.

$$u_C^m = n(t)u_C^{\Sigma}(t) \tag{3}$$

$$\frac{du_C^{\Sigma}(t)}{dt} = \frac{i(t)}{C^m} \quad with \quad C^m = \frac{C^{arm}}{n(t)} \tag{4}$$

With reference to Fig. 8, where only one phase is considered, it is possible to write a set of equations for currents: currents from upper and lower arms, rispectively i_U and i_L, will constitute the output current i_V.

The i_{diff} current represents the current that circulates from the phase leg to the DC link (and/or to another phase leg).

$$\left.\begin{aligned} i_U &= \frac{i_V}{2} + i_{diff} \\ i_L &= \frac{i_V}{2} - i_{diff} \end{aligned}\right\} \begin{aligned} i_V &= i_U + i_L \\ i_{diff} &= \frac{i_U - i_L}{2} \end{aligned} \tag{5}$$

These equations are representing the ideal condition in wich the contributions of upper and lower arms to the output current are equal. The difference current is introduced to consider the possible situation in which the capacitors are not equally charged to the reference value. In this MMC configuration the sum of all capacitor voltages of one arm is assumed to be equal to the DC Voltage u_D.

Equations (6) and (7) are the same of (4), just emphasizing the contributions of upper and lower arms in terms of voltage and current.

$$\frac{du_{CU}^{\Sigma}(t)}{dt} = \frac{n_U i_U}{C^{arm}} \tag{6}$$

$$\frac{du_{CL}^{\Sigma}(t)}{dt} = -\frac{n_L i_L}{C^{arm}} \tag{7}$$

With all these equations and the semplified circuit shown in Fig. 8, it is possible to write equations (8) and (9) as simple Kirkhoff voltage equations.

$$\frac{u_D}{2} - Ri_U - L\frac{di_U}{dt} - n_u u_{CU}^{\Sigma} = u_V \tag{8}$$

$$-\frac{u_D}{2} - Ri_L - L\frac{di_L}{dt} + n_L u_{CL}^{\Sigma} = u_V \tag{9}$$

Subtracting equation (9) to (8), and substituting the following equations

$$i_U - i_L = 2i_{diff}$$

$$\frac{di_U}{dt} - \frac{di_L}{dt} = 2\frac{di_{diff}}{dt} \tag{10}$$

it is possible to obtain this dynamic equation of the current i_{diff} :

$$\frac{di_{diff}}{dt} = \frac{u_D}{2L} - \frac{R}{L}i_{diff} - \frac{n_U}{2L}u_{CU}^{\Sigma} - \frac{n_L}{2L}u_{CL}^{\Sigma} \tag{11}$$

From equations (6) and (7), substituting i_U and i_L with the expressions given in (5), two dynamic equations of upper and lower arm voltages are obtained:

$$\frac{du_{CU}^{\Sigma}}{dt} = \frac{n_U}{C^{arm}}i_{diff} + \frac{n_U}{2C^{arm}}i_V$$

$$\frac{du_{CL}^{\Sigma}}{dt} = +\frac{n_L}{C^{arm}}i_{diff} - \frac{n_L}{2C^{arm}}i_V \tag{12}$$

From (12) it can be noted that with i_{diff} equal to zero, the load current acts in order to unbalance the upper and lower arm voltages. In steady state conditions the load current is changing assuming positive and negative values, then, the time derivative of the arm voltages are also changing, and in ideal conditions the arm voltage should oscillate around a constant mean value. The presence of non idealities and losses may lead the converter to be unstable. As a consequence, it can be concluded that only the presence of a suitable difference current allows the converter to operate correctly.
Using (11) and (12), a dynamic and continuous model is thus obtained and shown in (13).

$$\frac{d}{dt}\begin{bmatrix} i_{diff} \\ u_{CU}^{\Sigma} \\ u_{CL}^{\Sigma} \end{bmatrix} = \begin{bmatrix} -\frac{R}{L} & -\frac{n_U}{2L} & -\frac{n_L}{2L} \\ \frac{n_U}{C^{arm}} & 0 & 0 \\ \frac{n_L}{C^{arm}} & 0 & 0 \end{bmatrix} \begin{bmatrix} i_{diff} \\ u_{CU}^{\Sigma} \\ u_{CL}^{\Sigma} \end{bmatrix} + \begin{bmatrix} \frac{u_D}{2} \\ \frac{n_U i_V}{2C^{arm}} \\ -\frac{n_L i_V}{2C^{arm}} \end{bmatrix} \tag{13}$$

Assuming that a sinusoidal output voltage is desired, the reference signal for modulation is

$$m(t) = \widehat{m}\cos(\omega_N t) \tag{14}$$

and the ideal terminal voltage is given by

$$u_V(t) = \frac{u_D}{2} m(t) \tag{15}$$

In order to solve the system of equations (13) the load current should be known. Here, the following alternating current is assumed as the output load current

$$i_V(t) = \widehat{\imath_V}(t)\cos(\omega_N t + \varphi) \tag{16}$$

Where φ is the load phase angle and is arbitrary.
Using the reference signal in (14), the modulation indices for upper and lower arms can be expressed as

$$n_U(t) = \frac{1 - m(t)}{2} \tag{17}$$

$$n_L(t) = \frac{1 + m(t)}{2} \tag{18}$$

It can noted that the sum of upper and lower modulation indexes is always equal to 1. As a consequence, assuming the capacitor voltages of all modules equal to the refernce value, the sum of the voltages of upper and lower arms is always equal to the DC voltage u_D.
In real operating conditions the capacitor voltages will not be exactly equal to the reference value and as a result a difference voltage will be present forcing a difference current to flow between the leg and the DC source. A suitable control of this current is crucial for achieving a correct operation of the converter and an equal sharing of the DC voltage among all modules.
A possible control strategy is the one based on adding an offset voltage to upper and lower arm voltages u_{CU} and u_{CL} defined trough (17) and (18). This offset voltage (u_{diff}) is determined with some criteria aimed to keep the module voltages as close as possible to the reference value or to keep the energy stored in upper and lower capacitors equalized.
It will be shown in the next section that u_{diff} will not affect the terminal voltage (as u_V is related to the difeerence between upper and lower arm voltages), but will impact on i_{diff} current instead.

The number of levels that can be obtained depends on the assumptions made for the analysis. When assuming a constant DC voltage, actually it is possible to generate output voltages having a number of levels equal to 2N+1, whereas the number of levels must be reduced to N+1 if the the DC voltage has to be kept under control by the converter itself.
This is the situation that occurs in HVDC systems composed by two MMCs connecting the two ends of a DC cable. In this case there is no DC capacitor between the DC voltage terminals and a DC voltage controller is necessary. In this analysis a constant DC voltage will be assumed as the aim is to develop a strategy for keeping under control the total energy stored in each leg and the unbalance between the energy stored in upper and lower arms.

3.2 - Control Strategy

By adding and subtracting equations (9) to (8), it is possible to obtain two equations that clearly explain-a possible approach to MMC control:

$$u_V = \frac{u_{CU} - u_{CL}}{2} - \frac{R}{2} i_V - \frac{L}{2} \frac{di_V}{dt} \tag{19}$$

$$L \frac{di_{diff}}{dt} + R i_{diff} = \frac{u_D}{2} - \frac{u_{CL} + u_{CU}}{2} \tag{20}$$

As suggested in [8], from (19) and (20) is possible to draw the following conlcusion:

- the output voltage u_v depends only on the current i_V and on the difference between upper and lower voltage u_{CU}, u_{CL}
- the arm voltage difference acts like an inner alternating voltage, R and L as a passive inner impedence for alternating current
- i_{diff} depends only on the DC link voltage and the sum of arm voltages

Therefore it is possible to note that adding the same quantity to both arm voltages will not affect the AC side, but will influence the difference current instead, wich can thus be controlled.
It is opportune for control purposes to obtain an expression of upper and lower arm voltages in wich this voltage difference is included. Starting from (8) and substituting the upper current with

$$i_U = \frac{i_V}{2} + i_{diff}$$

leads to

$$\frac{u_D}{2} - \frac{R}{2} i_V - R i_{diff} - \frac{L}{2}\frac{di_V}{dt} - L\frac{di_{diff}}{dt} - u_{CU} = u_V \qquad (21)$$

(21) can be rewritten as

$$u_{CU} = \frac{u_D}{2} - u_V - \frac{R}{2} i_V - \frac{L}{2}\frac{di_V}{dt} - R i_{diff} - L\frac{di_{diff}}{dt} \qquad (22)$$

Considering that form (19)

$$u_V + \frac{R}{2} i_V + \frac{L}{2}\frac{di_V}{dt} = \frac{u_{CL} - u_{CU}}{2} = e_V \qquad (23)$$

(22) can be rewritten as

$$u_{CU} = \frac{u_D}{2} - e_v - u_{diff} \qquad (24)$$

The same development can be carried out for u_{CL} yielding

$$u_{CL} = \frac{u_D}{2} + e_v - u_{diff} \qquad (25)$$

where u_{diff} is defined as

$$u_{diff} = R i_{diff} + L\frac{di_{diff}}{dt} \qquad (26)$$

Equations (24) and (25) show how the difference voltage contribute to the reference values of upper and lower arm voltages.
The quantity e_v defined as

$$\frac{u_{CL} - u_{CU}}{2} = e_V \qquad (27)$$

is practically representing the output voltage u_v, apart from the voltage drop across R and L as shown in (19). So, in the following, e_v is used to represent the output voltage u_v.

In order to determine a possible control strategy for determining u_{diff}, it is opportune to introduce the energy stored in upper and lower arm capacitors.

Assuming that voltage and thus energy stored in each arm is equally shared between sub-modules, the upper and lower energy are

$$W_{CU}^{\Sigma} = N\left[\frac{C}{2}\left(\frac{u_{CU}^{\Sigma}}{N}\right)^2\right] = \frac{C}{2N}(u_{CU}^{\Sigma})^2 = \frac{C^{arm}}{2}(u_{CU}^{\Sigma})^2 \tag{28}$$

$$W_{CL}^{\Sigma} = N\left[\frac{C}{2}\left(\frac{u_{CL}^{\Sigma}}{N}\right)^2\right] = \frac{C}{2N}(u_{CL}^{\Sigma})^2 = \frac{C^{arm}}{2}(u_{CL}^{\Sigma})^2 \tag{29}$$

Considering now power equations of both upper and lower arms, it is possible to write:

$$\frac{dW_{CU}^{\Sigma}}{dt} = i_U u_{CU} = \left(\frac{i_V}{2} + i_{diff}\right)\left(\frac{u_D}{2} - e_V - u_{diff}\right) \tag{30}$$

$$\frac{dW_{CL}^{\Sigma}}{dt} = -i_L u_{CL} = \left(-\frac{i_V}{2} + i_{diff}\right)\left(\frac{u_D}{2} + e_V - u_{diff}\right) \tag{31}$$

The total capacitor energy in the leg and the difference capacitor energy between upper and lower arms are

$$W_C^{\Sigma} = W_{CU}^{\Sigma} + W_{CL}^{\Sigma} \tag{32}$$

$$W_C^{\Delta} = W_{CU}^{\Sigma} - W_{CL}^{\Sigma} \tag{33}$$

Differentiating (32) and (33), and introducing (30) and (31) yields

$$\frac{dW_C^{\Sigma}}{dt} = \left(u_D - 2u_{diff}\right)i_{diff} - e_V i_V \tag{34}$$

$$\frac{dW_C^{\Delta}}{dt} = \left(\frac{u_D}{2} - u_{diff}\right)i_V - 2e_V i_{diff} \tag{35}$$

These equations are very important to discuss the influence of i_{diff} on the total and difference capacitor energies. From (34), assuming i_{diff} having only a dc component its product with u_D represents the power delivered to the ac side (load and capacitors). The quantity u_{diff} i_{diff} represents the losses on the arm resistance R and the magnetic energy variation in the arm inductance L, $e_V i_V$ is the load power. So, a DC component of i_{diff} can be used to control the total capacitor energy.

From (35), it can be noted that a DC component of i_{diff} has no impact on the difference capacitor energy as there are no dc components in e_v. The conclusion is that the DC component of i_{diff} can only be used for controlling the total capacitor energy stored in the converter leg.

On the other hand, an alternating component of i_{diff}, having the same fundamental frequency as the output voltage e_v, could be usefully employed to control the distribution of the capacitor energy between upper and lower arms. In fact, the product e_v i_{diff} has a dc component that can be used to force the energy difference to change. A similar effect is created by u_{diff} i_V, but this quantity should be smaller for small value of R and L, thus in the following the control strategy will be developed with reference to the quantity e_v i_{diff} only.

3.3 - Consideration about Control Strategy and Model

It is necessary to make an important remark: the equations wrote and discussed in previous section lead to a continuous model, suitable for analysis and understanding of operation principle of the MMC. On the other hand, from the control point of view, these equations are not easy to use: even if it is possible to decouple continuous and alternate component of differential current, in order to properly track references, non-linear couplings make really complex advanced control structures.

From equations (34) and (35) it becomes clear that the input variables, or rather modulation indexes, influence dynamics of the energy as a non-linear input: in fact, the modulation indexes directly influence differential voltage, and the relationship between differential voltage and differential current is a low-pass filter (Fig. 10).

Figure 10 - Input Control Relationship

Neglecting this low pass filter it is possible to consider that input variables are a "square" input for the system: this condition makes more difficult the development of advanced control strategies and the study of complex control strategies.
Thus, a different approach in the modeling will be developed in order to simplify the analysis from the control point of view: this modeling approach will be deepened in Chapter V.
The control strategy implemented is a linear control which aims to operate in the proximity of the region where the control can be considered linear: actually, control input will be limited in order to preserve this assumption. Otherwise, the non-linear input of the control can affect operation of the system, leading to instability.
Two different loops will be implemented, the first one to control the overall energy of the MMC leg, the second to control the balance between upper and lower arms of the phase-leg.
The interaction between two loops may lead to instability: because of the non-linear configuration of system equations, it is hard to analyze systems coupling properly (for instance Relative Gain Array analysis).
It is however evident that total energy and energy balance interact dynamically in system operation: in order to make a decoupling, balance of energy loop is tuned in order to be greatly slower than the overall energy loop. This frequency decoupling will highly benefit differential current waveform: if not performed, overall energy and balance interaction leads to a really distorted differential current. This current, flowing in the phase-leg, would produce a voltage drop on the phase impedance, increasing losses and disturbances in the stability of the system.
Then, an output current control loop will be implemented in order to simulate the operation of the converter in all different possible conditions. The general block diagram of control scheme is shown in Fig. 11.

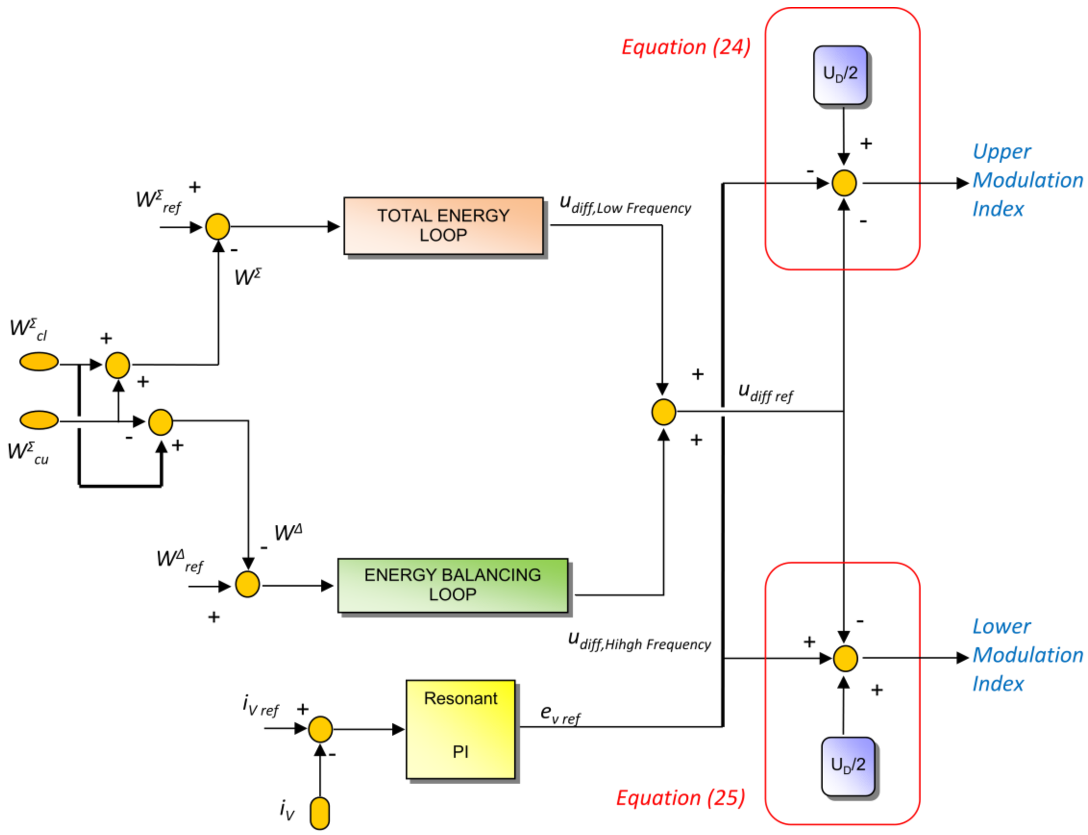

Figure 11 - Control Scheme, Block Diagram

Chapter IV

4.1 - Development of a MATLAB model

Starting from equations and discussions of Chapter III, it is possible to define a simple dynamic model of one phase of the converter.
Below are listed the chosen equations:

$$\frac{d}{dt}\begin{bmatrix} i_{diff} \\ u_{CU}^{\Sigma} \\ u_{CL}^{\Sigma} \end{bmatrix} = \begin{bmatrix} -\frac{R}{L} & -\frac{n_U}{2L} & -\frac{n_L}{2L} \\ \frac{n_U}{C^{arm}} & 0 & 0 \\ \frac{n_L}{C^{arm}} & 0 & 0 \end{bmatrix} \begin{bmatrix} i_{diff} \\ u_{CU}^{\Sigma} \\ u_{CL}^{\Sigma} \end{bmatrix} + \begin{bmatrix} \frac{u_D}{2} \\ \frac{n_U i_V}{2C^{arm}} \\ -\frac{n_L i_V}{2C^{arm}} \end{bmatrix} \tag{13}$$

$$\frac{dW_{CU}^{\Sigma}}{dt} = i_U u_{CU} = \left(\frac{i_V}{2} + i_{diff}\right)\left(\frac{u_D}{2} - e_V - u_{diff}\right) \tag{30}$$

$$\frac{dW_{CL}^{\Sigma}}{dt} = -i_L u_{CL} = \left(-\frac{i_V}{2} + i_{diff}\right)\left(\frac{u_D}{2} + e_V - u_{diff}\right) \tag{31}$$

$$\frac{di_V}{dt} = \frac{u_V}{L_g} - \frac{u_g}{L_g} - \frac{R_g}{L_g} i_V \tag{36}$$

Equation (36) is the output voltage equation, where u_g is the grid voltage, and R_g, L_g the parameters of the line connecting MMC to the grid.
The previous equations are implemented on Simulink, with the use of Embedded MATLAB Functions.

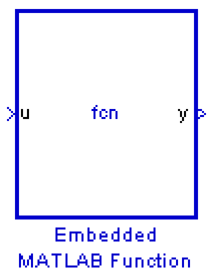

4.2 - First model: Converter Operation and Model Verification

The first system implemented in MATLAB-Simulink includes only the equations in (13), but it is however important to understand the operation of the converter: in particular, the necessity of controlling the differential current and thus the energy stored in upper and lower arm becomes clear.
In this simulation, output voltage and current are imposed and the operation of the system is then observed: modulation indexes are calculated ideally, using equations (24) and (25), neglecting differential voltage usage (no control strategy is implemented yet) and neglecting also the voltage drop of the output current on the arm parameters (i.e. $u_V = e_v$).

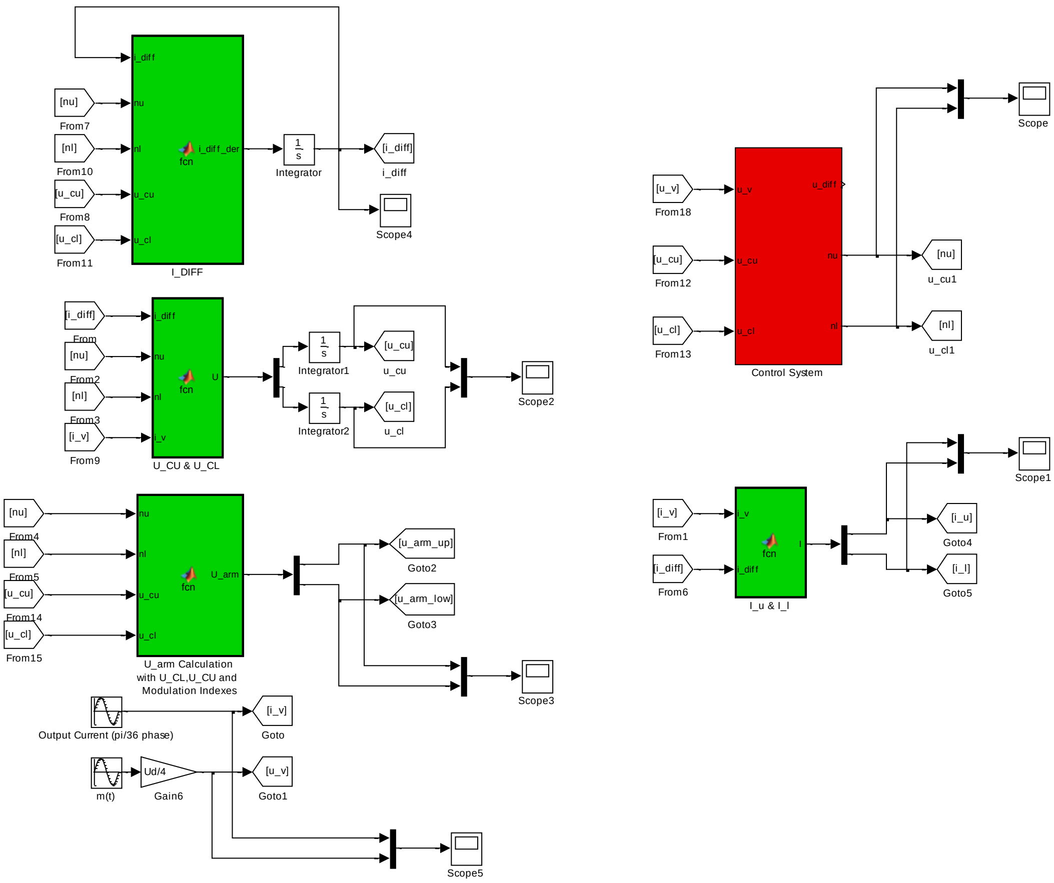

Figure 12 - First Model MATLAB Scheme

MATLAB Model Implementation can be seen in Fig. 12.
Green blocks implement model equations; the red block instead contains the calculation of the modulation indexes: in the right bottom, output voltage and current are imposed, assuming a load-phase angle equal to zero.

The upper green block represents the dynamic of differential current; the middle green block represents the capacitor voltage dynamic, the lower block calculates the upper and lower arm voltage, multiplying the capacitor voltage by the modulation index. On the right side, the green block is used to calculate the upper and lower arm current. Output voltage and current, and other system parameters are listed below in Tab. 1.

$u_V = 50\ \sin(\omega t)\ \ V$
$i_V = 10\sin(\omega t + \varphi)\ \ A$
$f = 50\ Hz$
$\varphi = 0$
$u_D = 200\ \ V$
$u_{CU}^{\Sigma}(ref) = 200\ V$
$u_{CL}^{\Sigma}(ref) = 200\ V$
$C^{arm} = 5\ \ mF$
$R = 0.1\ \Omega$
$L = 3\ \ mH$

Tab. 1 – List of system parameters

It is important to underline that the model implemented is a kW system: the choice to preliminary study a smaller system, compared with the final objectives of project, is motivated by control issues and parameters availability.

It will be shown that control strategy implemented is almost independent from parameters changes; however it is easier to start solving the problem from a small scale system. Furthermore, parameters for a kW system were available from the beginning of the project, instead MW parameters required some time and deepening to be confirmed.

No control loop is implemented yet, and the converter is not able to keep the capacitor voltage to the initial value, i.e. the capacitor voltage decreases from the initial value to a non-desired “steady state condition”, the same happens to differential current.

Arm voltages waveforms are shown in Fig. 13.

After a brief transient the differential current acts in order to maintain the capacitor voltage stable (waveform in Fig. 14), and the system is operating properly.

In order to control the capacitor voltage and thus totla energy stored in upper and lower arm, and their balance, a control on the differential current must be implemented.

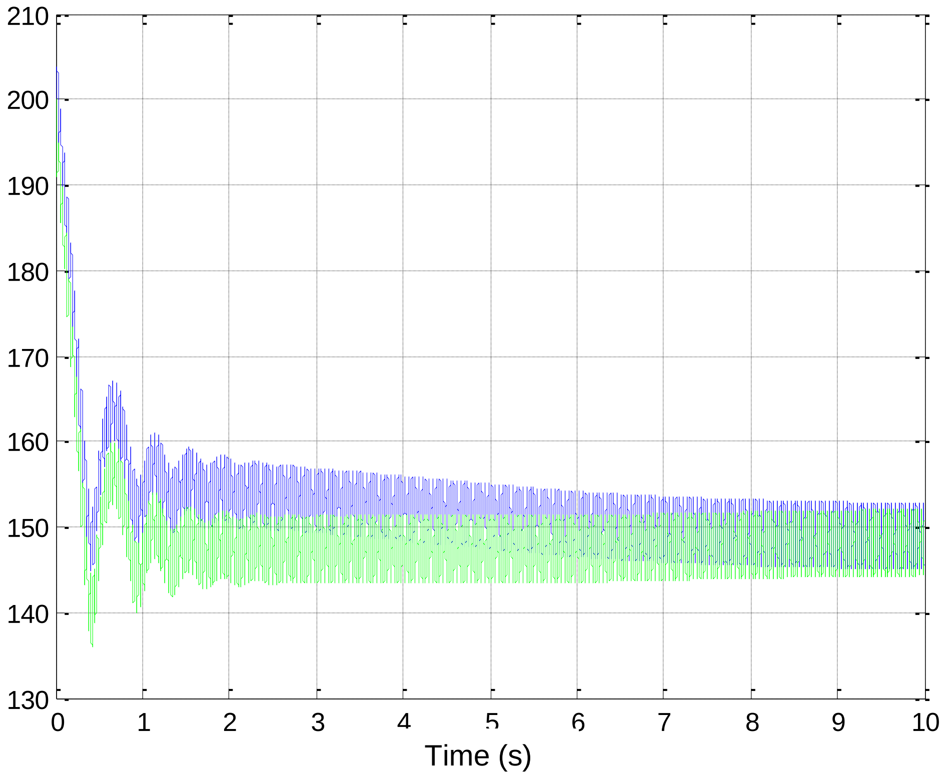

Figure 13 – Upper (Blue) and Lower (Green) Arm Capacitance Voltage (V): without control loop

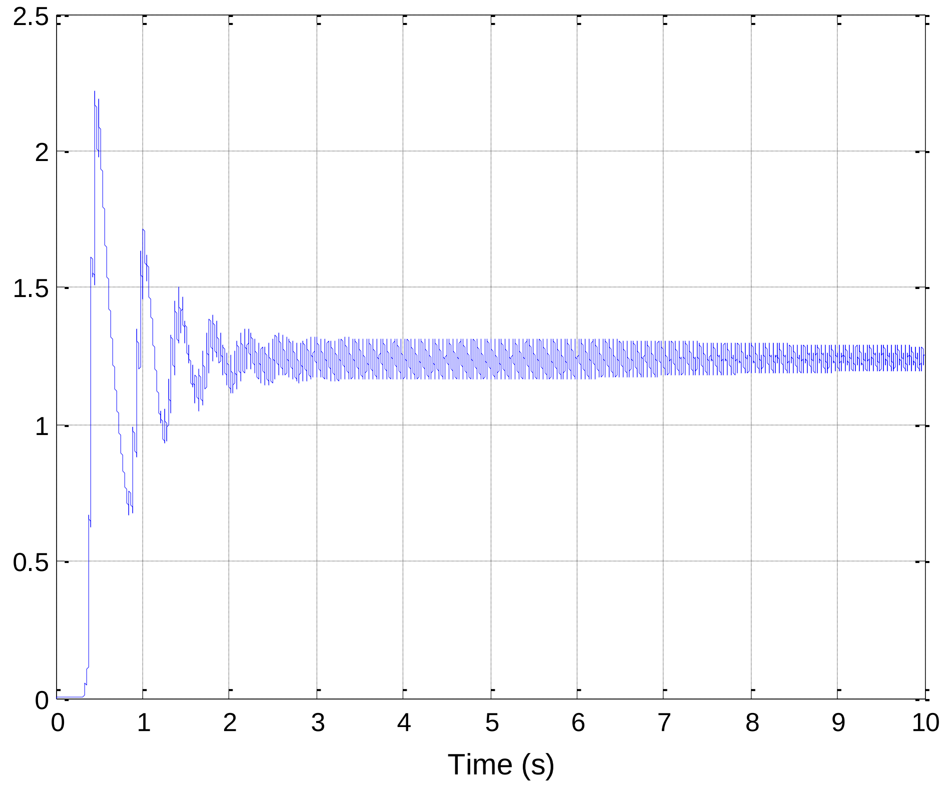

Figure 14 - Differential Current Waveform (A): without control loop

4.3 - Second model: Energy Control

The second system implemented includes energy equations (30) and (31) and propose an energy control strategy, to obtain a stable single-phase leg of the converter: to accomplish this, differential current is used. Like the previous model, output voltage and current are still imposed and the operation of the converter-leg is consequently observed and controlled.

As deducted by equations (19) and (20), differential current can be controlled by a differential; this voltage will not affect the AC (output) side (i.e. adding the same quantity to upper and lower arm voltage does not change the output current or voltage, but imposes a differential current to flow in the phase-leg).

Thus, a simple but efficient control strategy controls overall energy stored and the balance between upper and lower arm energy through the differential current, using the differential voltage as intermediate control input: in fact this differential voltage, sum of two different control components, will modify modulation indexes, changing the ideal value calculated assuming constant the capacitor voltages.

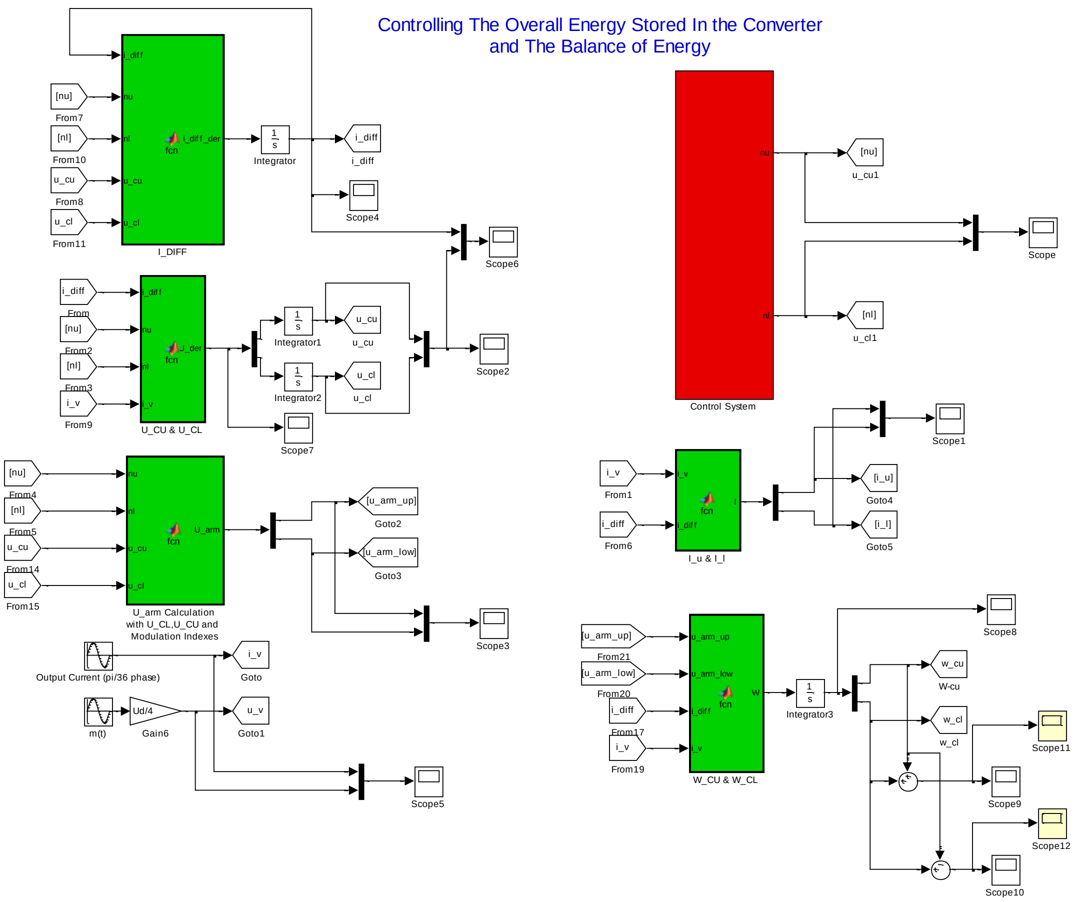

Figure 15 - Second Model MATLAB Scheme

Dynamic equations for upper and lower energy are implemented in the lower, right side MATLAB Embedded block: then, the sum of the two energies stored in upper and lower arms is the overall energy and a constant reference value is imposed. The difference of upper and lower arm energies is used to control the balance between upper and lower arm; thus, the reference value is set to zero. The control scheme block is then explained and can be seen in Fig. 16.

Red blocks implement the overall energy loop: a PD controller works on the total energy error, with the purpose of deleting the error between energy reference and the energy effectively stored in the phase-leg.

However, being all the imposed output signals sinusoidal, there will be a steady state error in the overall energy: the goal is to reduce this error as much as possible and to have a fast dynamic response in case of change reference.

Green blocks implement the balance control between upper and lower arm: it is again a PD controller, but this time a low pass filter is also required, in order to have a stable and smooth loop. The control action generated by this loop is then multiplied by a "carrier", with the same frequency of the output signals and the impedance arm phase.

From equations (34) and (35), rewritten in the following for convenience, it is possible to understand how to control properly the overall energy and the energy balance.

$$\frac{dW_C^{\Sigma}}{dt} = \left(u_D - 2u_{diff}\right)i_{diff} - e_V i_V \qquad (34)$$

$$\frac{dW_C^{\Delta}}{dt} = \left(\frac{u_D}{2} - u_{diff}\right)i_V - 2e_V i_{diff} \qquad (35)$$

In equation (34), differential current multiplies the DC voltage, so a DC component of differential current is used to control the overall energy stored.

In equation (35), differential current multiplies the output voltage (e_V can be considered the same of output voltage, neglecting the voltage drop of output current on arm parameters), so an AC component of differential current is used in order to control the balance between upper and lower energy (using the carrier technique implemented by the yellow block).

The two control components are added and then used as a differential voltage reference which will be followed by changing upper and lower modulation indexes, driving the necessary differential current to control the system energy: modulation indexes are calculated dividing the upper and lower voltage (calculated with equations (24) and (25)) by the capacitor voltage reference, as it is shown in the lower part of the control scheme with green blocks.

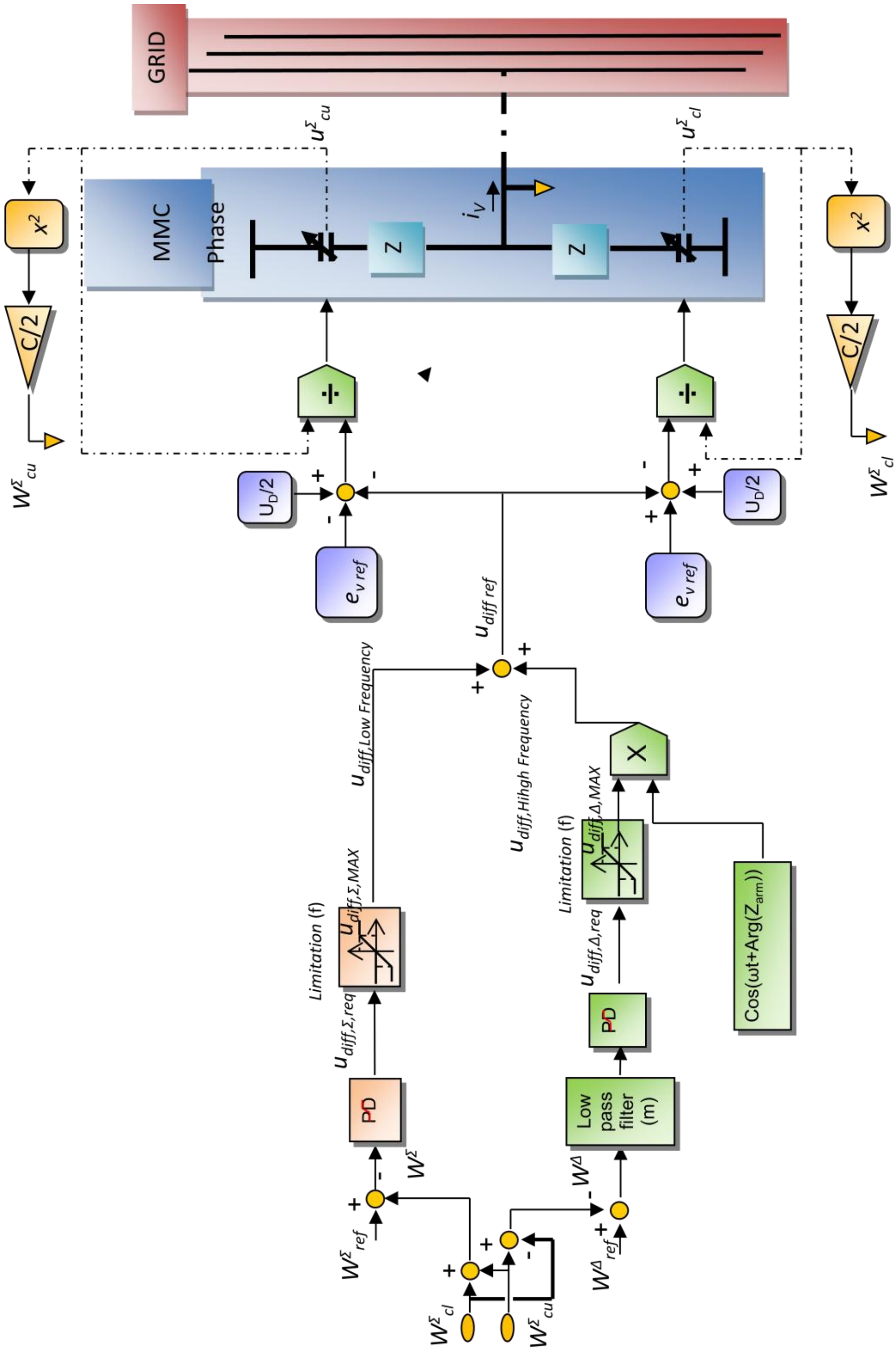

Figure 16 – Control Scheme Implementation in MATLAB

An important consideration must be performed: both loops implemented to control energy behavior include saturation. There are two important reasons in order to impose these limitations:

- Stability of the System: it is necessary to leave the control enough slack in order to properly act on the system. It is however important to remember the non-linear configuration of the input, which impose a strict constraint to input magnitude
- Output Tracking: this point will be shown clearly in the following model, Chapter 4.4, where output variables control is implemented. It is important to use a small percentage of voltage available to control energy: the remaining part is necessary to control the output.

4.3.1 - Simulation Results

Imposing the output current, the overall energy stored in one phase leg has a brief transient after which it oscillates around the steady state reference value: the amplitude of the oscillation is less than 1% and the frequency is the same of the output signals. The waveform is shown below, in Fig. 17.

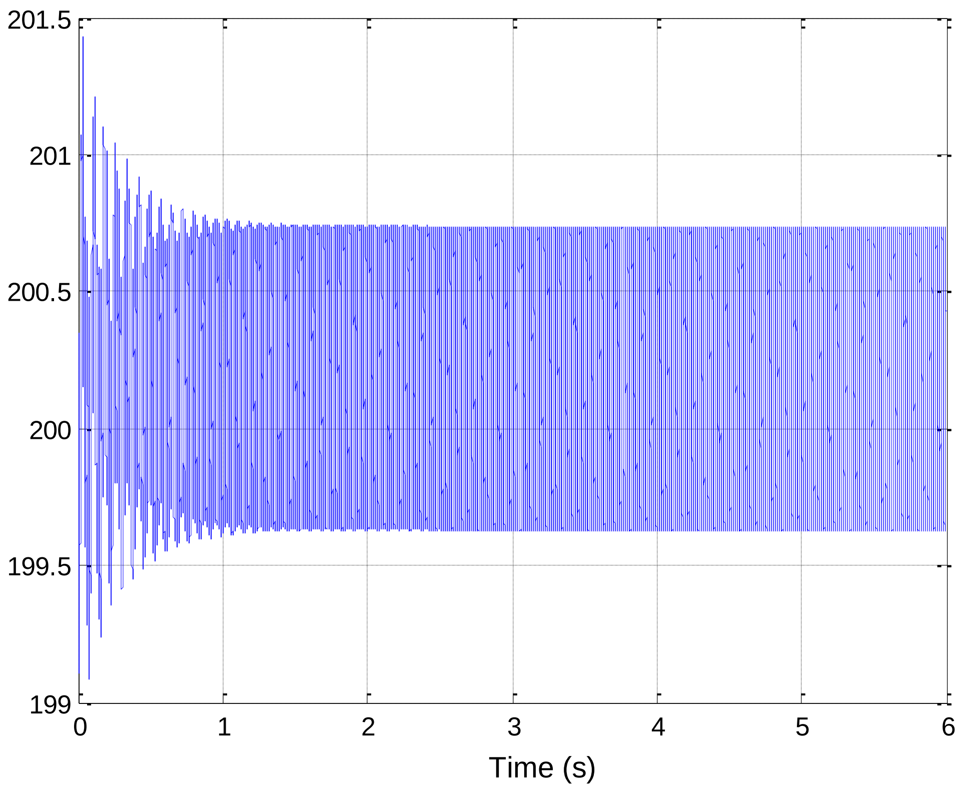

Figure 17 - Overall Energy Stored in the Converter Phase (Joule): steady-state condition of the overall energy in a converter phase

Initial transient is caused by the difficulty in finding a proper initial condition for the system: even if the capacitors are charged, also differential current has to be set to a proper value. Even if the mean value can be found, the alternate component of the differential current in order to balance energy/voltages requires a transient.
The energy difference between upper and lower arm has a similar behavior: after a brief transient, it reaches a steady state oscillation around the reference, 1% of amplitude compared to the overall energy value and with the same frequency of the output (Fig. 18).

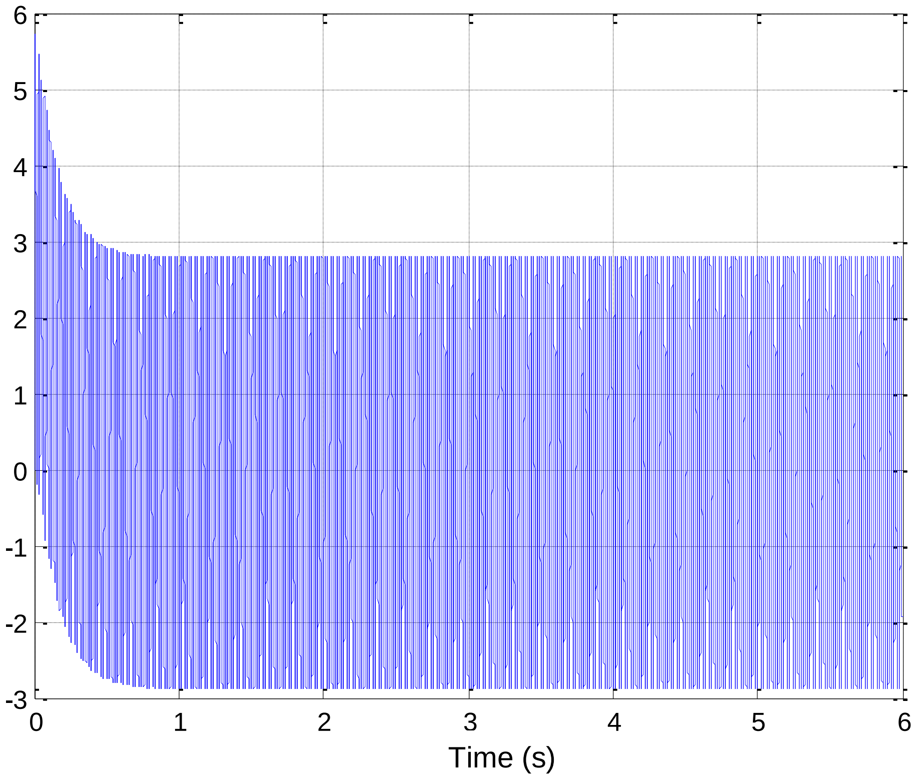

Figure 18 - Difference Between Upper and Lower Arm Energy (Joule): steady-state condition of the difference energy

The steady state behavior is stable as expected: some problems may occur, especially if dynamic changes of the energy are imposed.
In these cases, transient with oscillations are present and they will be discussed and deepened in coming sections.

4.4 - Third model: Output Power Control

With the third implemented model, the goal is to deepen the behavior of the converter about the output current control: proved the overall and balance energy control stability, it is now possible to introduce the control of the output current.

To track the output current, a resonant controller is used; a standard PI structure would be insufficient to cancel the sinusoidal error, so a different approach is necessary to be adopted. The resonant controller is the most suitable for a single-phase system: however, considering the three-phase general structure, a D-Q or Space Vector transform will be chosen for the control structure, in order to simplify the complexity of control loops.

A MATLAB Embedded block is added in order to implement the output current dynamic equation; then, a resonant controller is applied to output current error, as it is shown in Fig. 19. The controller is composed of two main contributions: a proportional, and a resonant part. The Bode diagram is shown below in Fig. 20. The resonant peak is in correspondence of the frequency of the output and can be changed dynamically in order to follow different outputs (in terms of frequency).

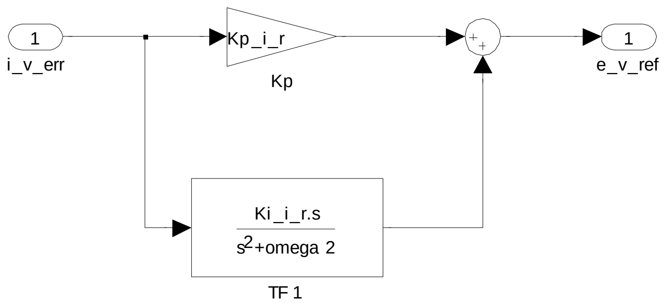

Figure 19 - Resonant Controller MATLAB Scheme

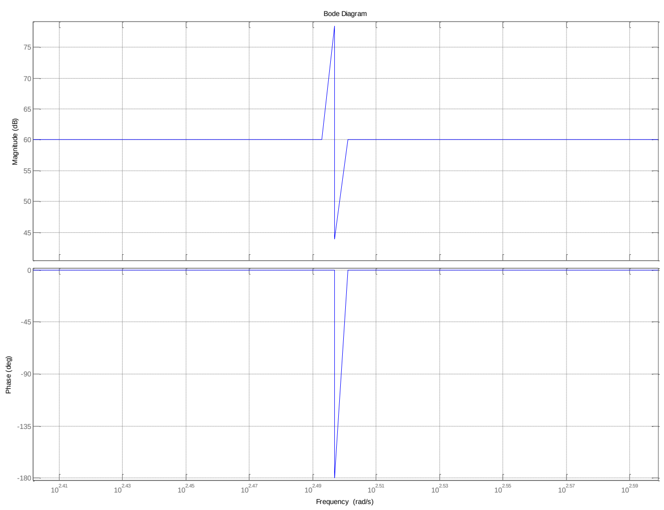

Figure 20 - Bode Diagram of Resonant Controller

The output of the resonant controller is a reference for the inner alternate voltage e_V, which again will be achieved through the control of modulation indexes.
The general scheme implemented in MATLAB for the third model is represented in Fig. 21.

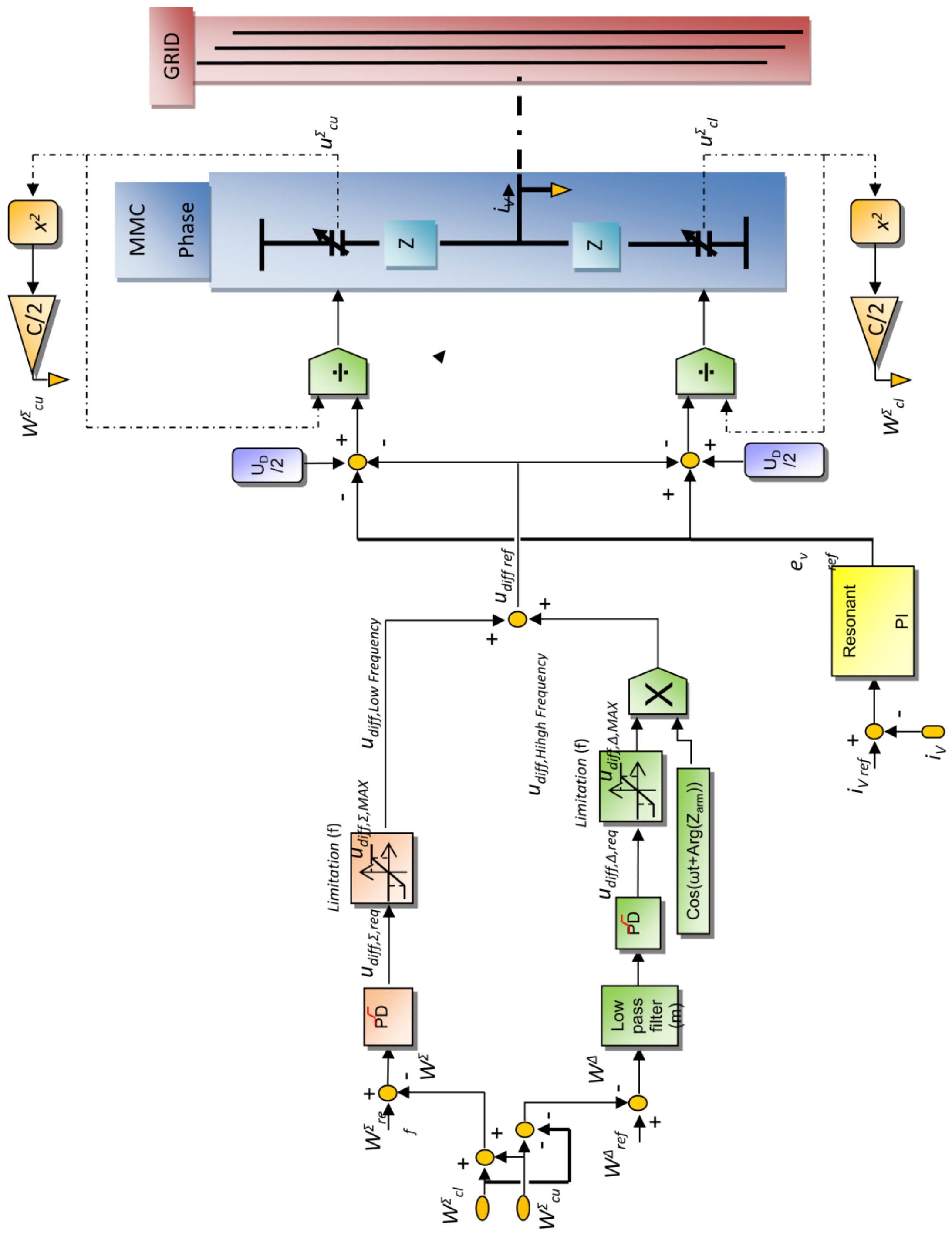

Figure 21 - Third Model MATLAB Control Scheme

4.4.1 - Simulation Results

Simulation results show that adding control loop for the output current does not impact the energy behavior of the system.

Both overall energy and the balance between upper and lower arm behave as shown in previous examples: thus, it is possible to consider that energy control and output current control are decoupled. This is possible because of saturation imposition: actually, limitations and constraints on differential voltage are important both for stability of the system and output variables tracking.

If tuned properly, the energy control system will use a small fraction of the DC voltage; the remaining part is used to guarantee the output tracking. Differential current control exploits only a small quantity of the voltage available; the rest is used to control the output.

If the trade-off between the energy control and output power control is properly tuned, energy loop and output loop can be considered decoupled.

Fig. 22, shows the behavior of differential current; the current has a DC component of 1.1 A, and an alternating component around 0.1 A of amplitude.

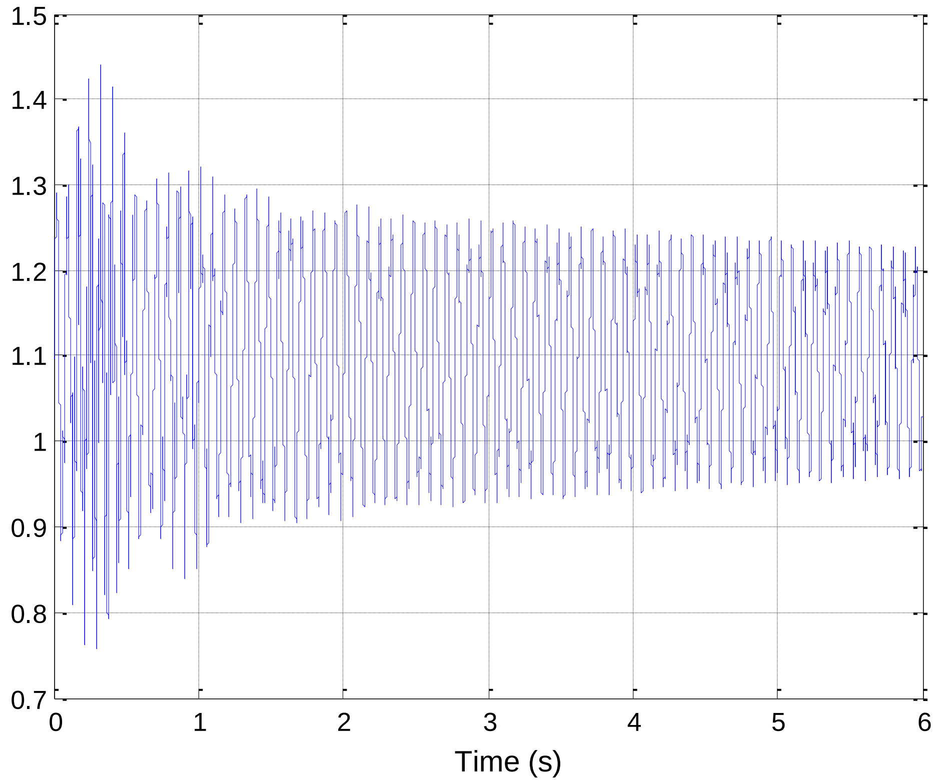

Figure 22- Differential Current Waveform (A)

The error of the output current is shown in Fig. 23; it is possible to see that, after a brief transient, the current reaches almost the desired value with an error less than 1% of the steady state value of the output current.

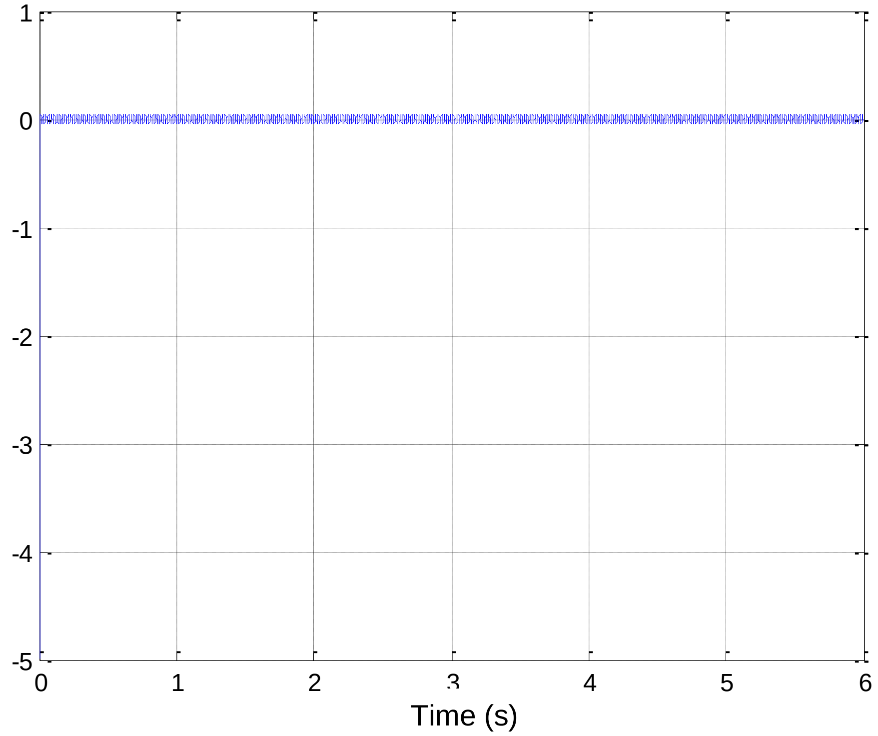

Figure 23 - Output Current Error (A)

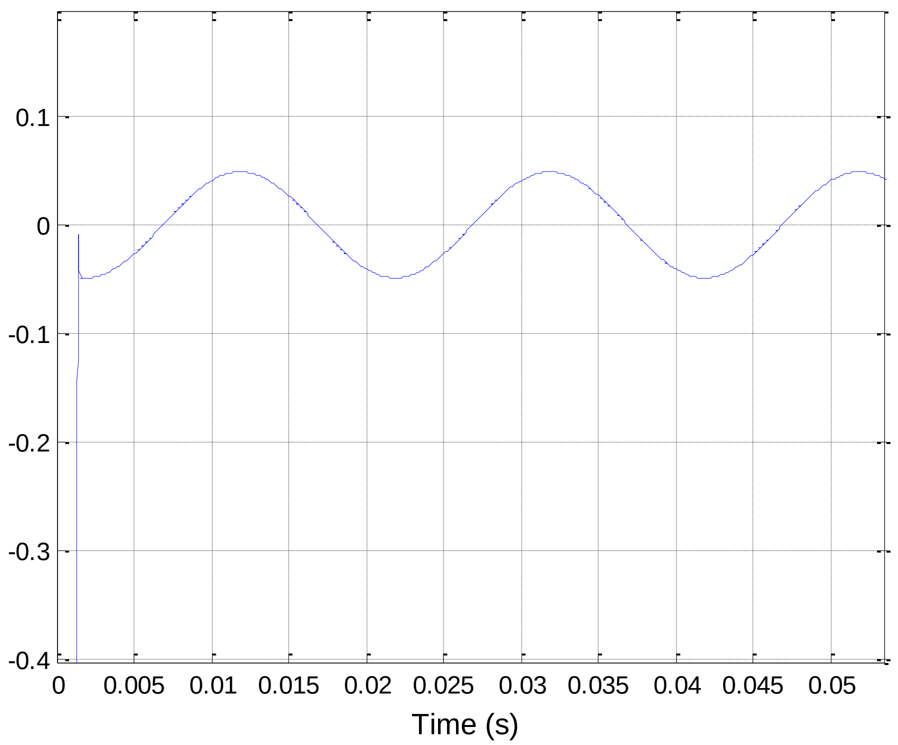

Figure 24 - Zoom of Output Current Error (A)

Fig. 24 shows a zoom of the fast transient of output current error, almost impossible to be seen in Fig. 23. The initial error is of course big (the output current starts form a null value), but after few milliseconds the error is less than 1% of the steady state value.

The dynamic behavior of the system needs to be investigated. To this aim, a dynamic change of the overall energy is imposed in order to show the behavior of the system.

The imposed change is not connected to any particular working situation; it is just used to show the dynamic response in time and damping, obtained with the control system. For instance, this increase of the overall energy may be related to a failure mode condition, considering the increase of energy a way to maintain the system stable even if a certain part of the converter is not working properly.

Simulation results, illustrated in Figs. 25 and 26, show the behavior in case of a simple proportional regulator: actually, is not a usually accepted operation response in dynamic systems. Even if the response itself is fast, the damping obtained with a proportional controller is not satisfying, especially in the overall energy control loop. These results call for a PD configuration of the controller: adding a derivative action, enough phase margin can be reached, in order to smooth the oscillation of the system.

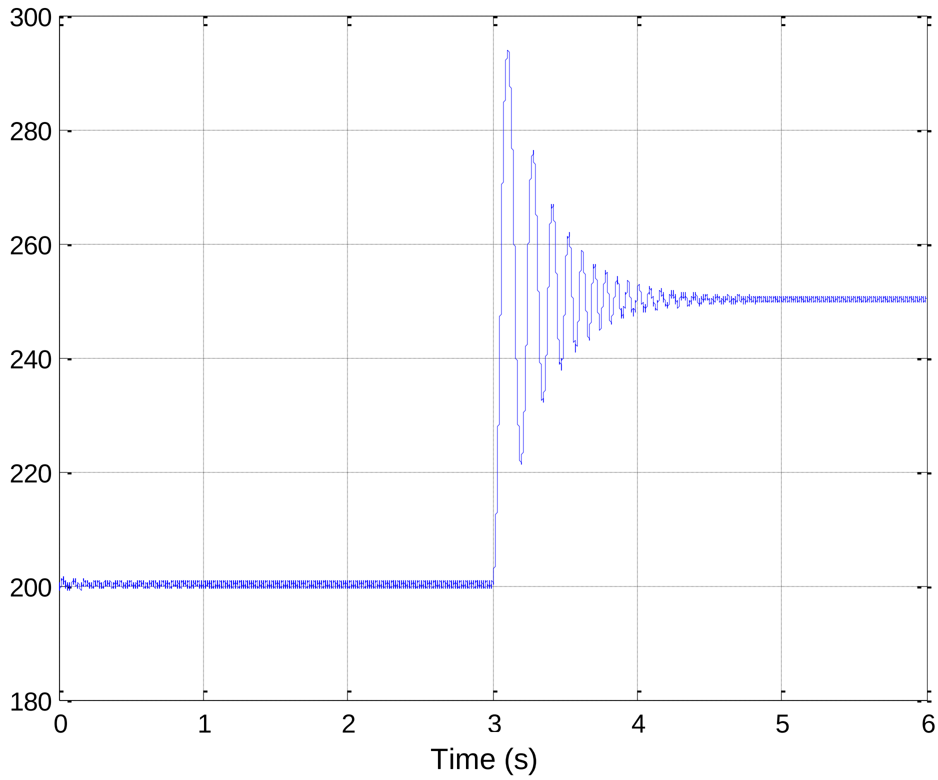

Figure 25 - Dynamic Response of Overall Energy Stored in Phase Leg (Joule): transient generated by a step-change in the overall energy reference

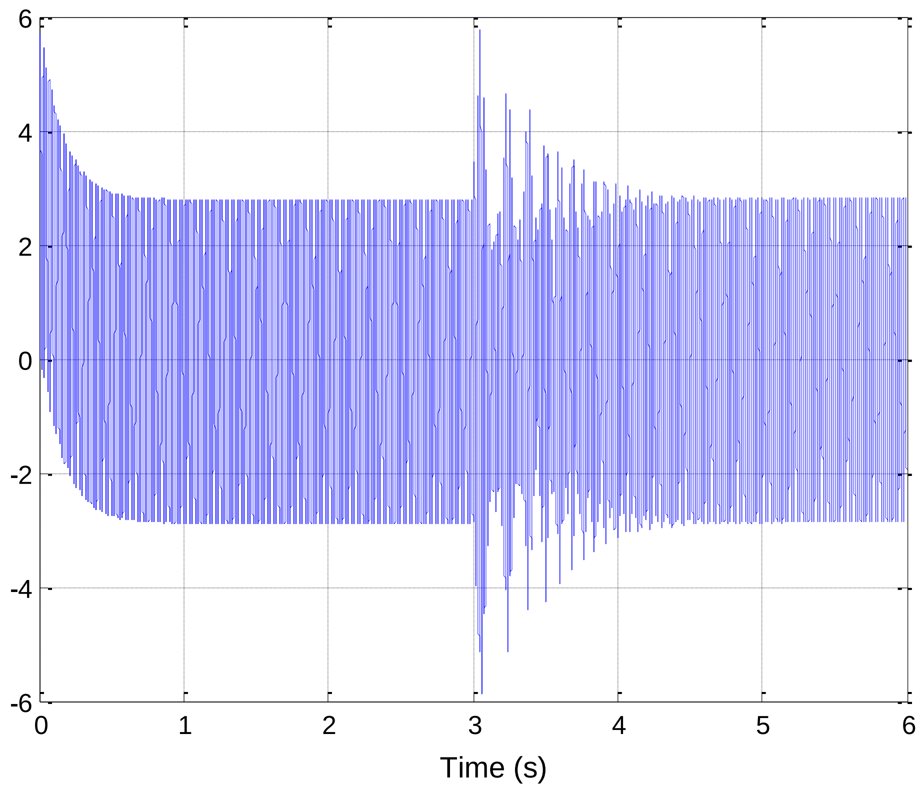

Figure 26 - Dynamic Response of the Difference between Upper and Lower Arm Energy (Joule): overall energy oscillations affect also the balance loop

Derivative action is underlined with red background in Fig. 27 and simulation results are shown in Figs. 28 and Fig. 29. Energy behavior improvements are evident and the control system now works as expected.

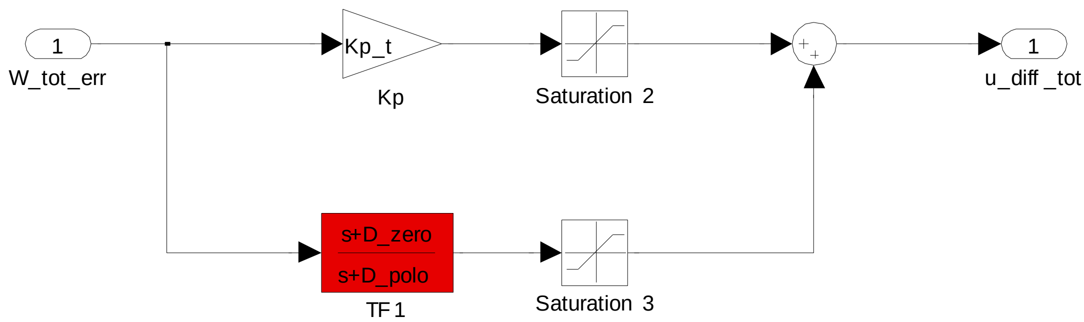

Figure 27 - Addition of Derivative Action in the Controller

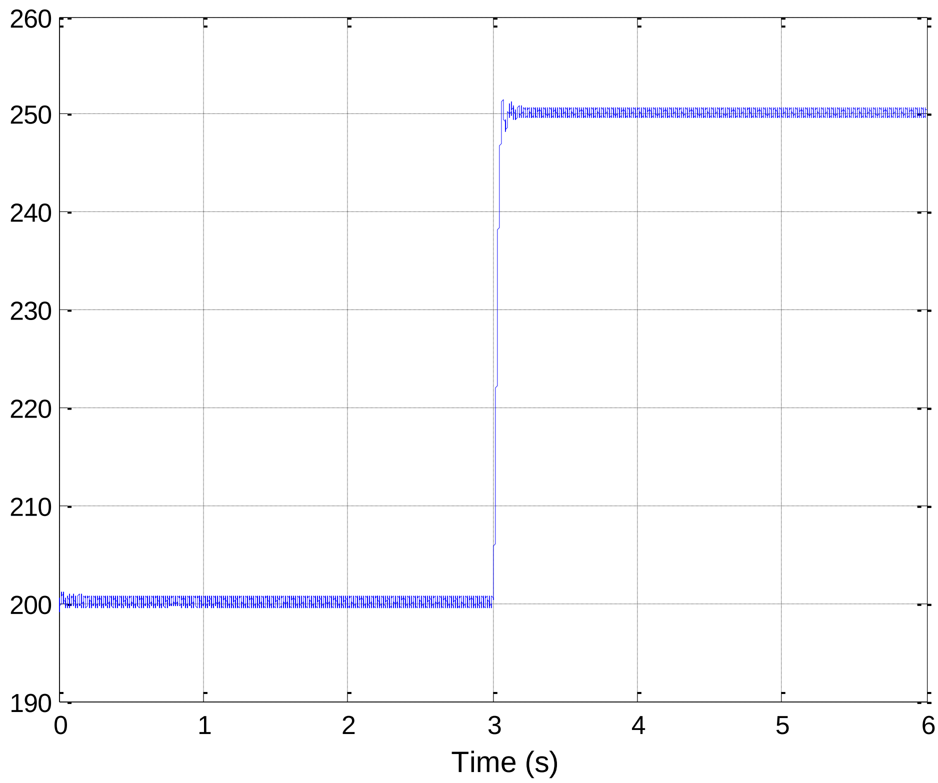

Figure 28 - Overall Energy Behavior with PID Regulator (Joule)

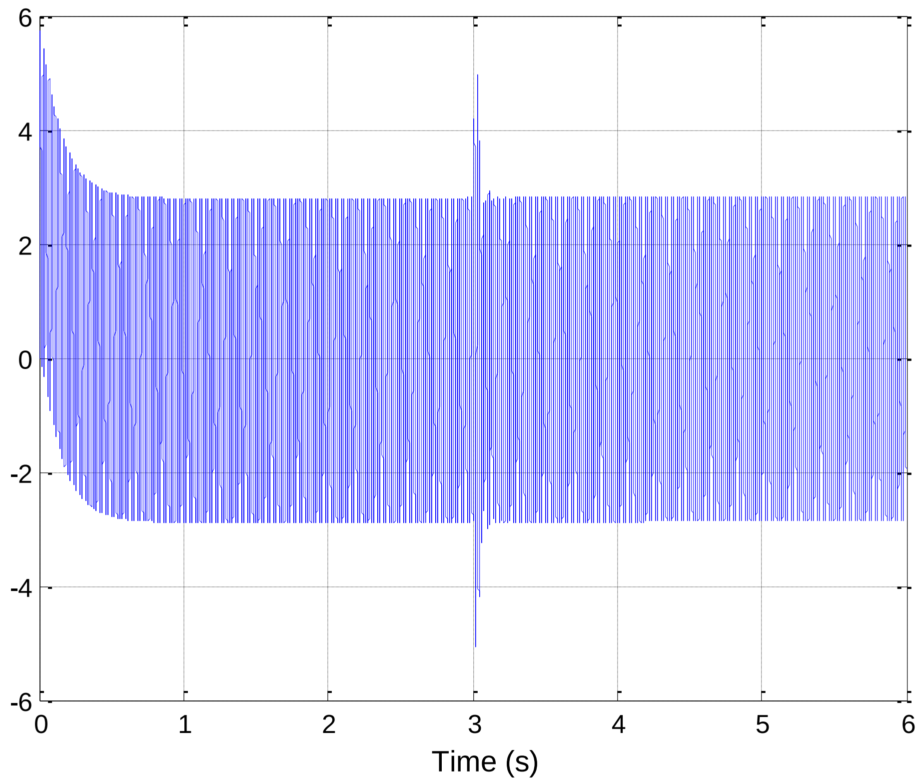

Figure 29 - Difference Energy with PID Regulator (Joule)

4.5 - Fourth model – Mega-Watt System

The model presented and studied in previous sections was a kW power system: in this chapter the analysis and simulation results will be proven on a MW power system.
The MW power system requires only changing the limitations on the differential voltage available: as much as the power increases, as much the differential voltage, used to control the energy stored in the system, has to increase.
The control system scheme remains exactly the same, and will be proven to be reliable and tightly dependent with system parameters: however, an important consideration has to be deepened about system project.
Even if not compromising stability, C^{arm} plays a fundamental role in the operation of the system: the sizing of this parameter has to take in consideration the voltage ripple that it's considered to be acceptable. When considering the previous simulations (the kW power system) C^{arm} was big enough in order to minimize voltage ripples in the upper and lower modules: considering a MW power system, it is important to discuss the size of the capacitor in order to understand the relationship between this parameter and control constraints.

4.5.1 - Capacitance - Voltage Ripple Relationship

Starting from voltage derivate equations in (13), here rewritten for convenience,

$$\frac{du_{CU}^{\Sigma}}{dt} = \frac{n_U}{C^{arm}} i_{diff} + \frac{n_U}{2C^{arm}} i_V$$

$$\frac{du_{CL}^{\Sigma}}{dt} = \frac{n_L}{C^{arm}} i_{diff} - \frac{n_L}{2C^{arm}} i_V \qquad (13)$$

it is possible to find a relationship between voltage and arm capacitance. Considering only the upper arm voltage (but same results would be obtained considering lower arm voltage), it is possible to substitute currents with their behavior over time

$$i_{diff} = I_0 \qquad (37)$$

$$i_V = I_M \sin(\omega t) \qquad (38)$$

For the differential current, it is possible to consider only the DC component: this component is used to maintain the capacitor voltage to a constant value.
It is possible to integrate the voltage equation in the positive half period of the output current, yielding

$$u_{cu}^{\Sigma} - u_{cu}^{0} = \frac{1}{C^{arm}} \int_0^{\pi} n_u [I_0 + I_M \sin(\omega t)]\, d(\omega t) \tag{39}$$

where modulation index con be considered as

$$n_U(t) = \frac{1 - m(t)}{2} \tag{40}$$

with the hypothesis that

$$m(t) = \sin(\omega t) \tag{41}$$

Substituting (40) and (41) in (39) we obtain

$$u_{cu}^{\Sigma} - u_{cu}^{0} = \frac{1}{C^{arm}} \int_0^{\pi} \left[I_0 \frac{1 - \sin(\omega t)}{2} + I_M \sin(\omega t) \frac{1 - \sin(\omega t)}{2} \right] d(\omega t) \tag{42}$$

$$u_{cu}^{\Sigma} - u_{cu}^{0} = \frac{1}{C^{arm}\omega} \left[\frac{I_0}{2} \pi - \frac{I_0}{2} [-\cos(\omega t)]_0^{\pi} + \frac{I_M}{4} [-\cos(\omega t)]_0^{\pi} \right] + \frac{1}{C^{arm}} \int_0^{\pi} \sin(\omega t)^2 \; d(\omega t) \tag{43}$$

$$u_{cu}^{\Sigma} - u_{cu}^{0} = \frac{1}{C^{arm}\omega} \left[\frac{I_0}{2} \pi - I_0 + \frac{I_M}{2} - \frac{I_M}{4} \frac{\pi}{2} \right] \tag{44}$$

Finally a relationship between C^{arm} and voltage ripple is found as

$$u_{cu}^{\Sigma} - u_{cu}^{0} = \frac{I_0 \left[\frac{\pi}{2} - 1 \right] - I_M \left[\frac{\pi}{8} - \frac{1}{2} \right]}{C^{arm}\omega} \tag{45}$$

With this equation it is possible to understand the system operation and thus to size properly the capacitance of the arm, once assigned output current and calculated the DC component of differential current, in order to satisfy voltage ripple constraints.

4.5.2 - Simulation Results

Parameters of Mega-Watt power system are listed in Tab. 2.

$u_g = 9 \sin(\omega t) \quad KV$
$R_g = 0.1 \ \Omega$
$L_g = 5 \quad mH$
$i_V = 1.5 \sin(\omega t + \varphi) \ \ kA$
$f = 50 \ Hz$
$\varphi = 0$
$u_D = 20 \ KV$
$u_{CU}^{\Sigma}(ref) = 20 \ KV$
$u_{CL}^{\Sigma}(ref) = 20 \ KV$
$C^{arm} = 5 \quad mF$
$R = 0.1 \quad \Omega$
$L = 30 \ \ mH$

Tab. 1 – List of system parameters

The first simulation shown in the report shows the steady state operating conditions of the MW power converter: as expected, the general behavior of the converter is unchanged in comparison with the kW power converter.

The only change can be seen in the order of magnitude of variables observed. Figs. 30 and 31 show total energy and balance energy waveforms.

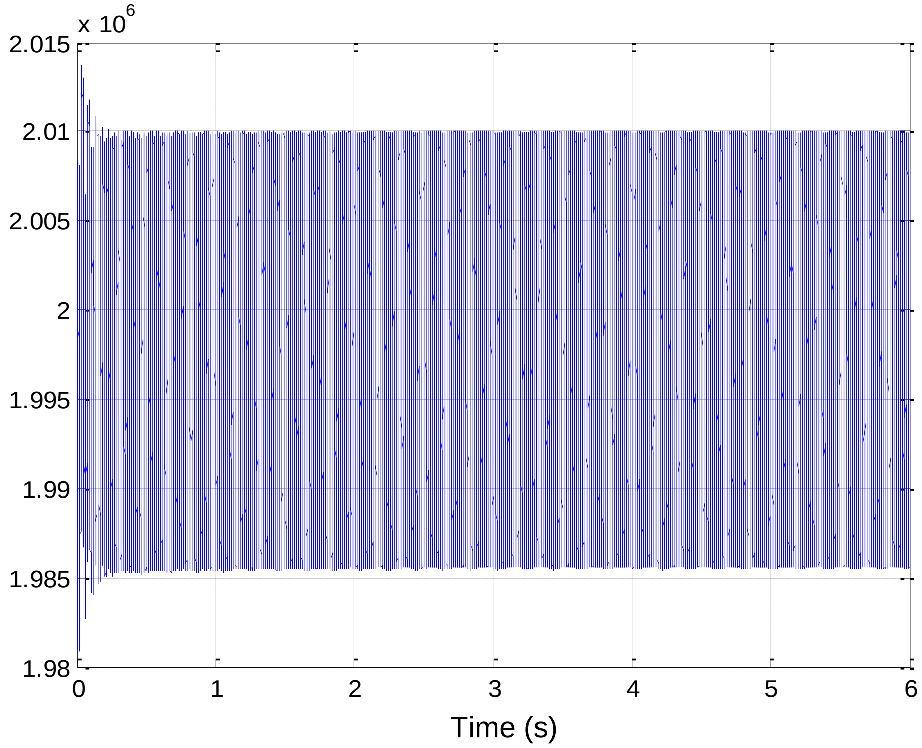

Figure 30 - Overall Energy (Joule) Steady State Waveform

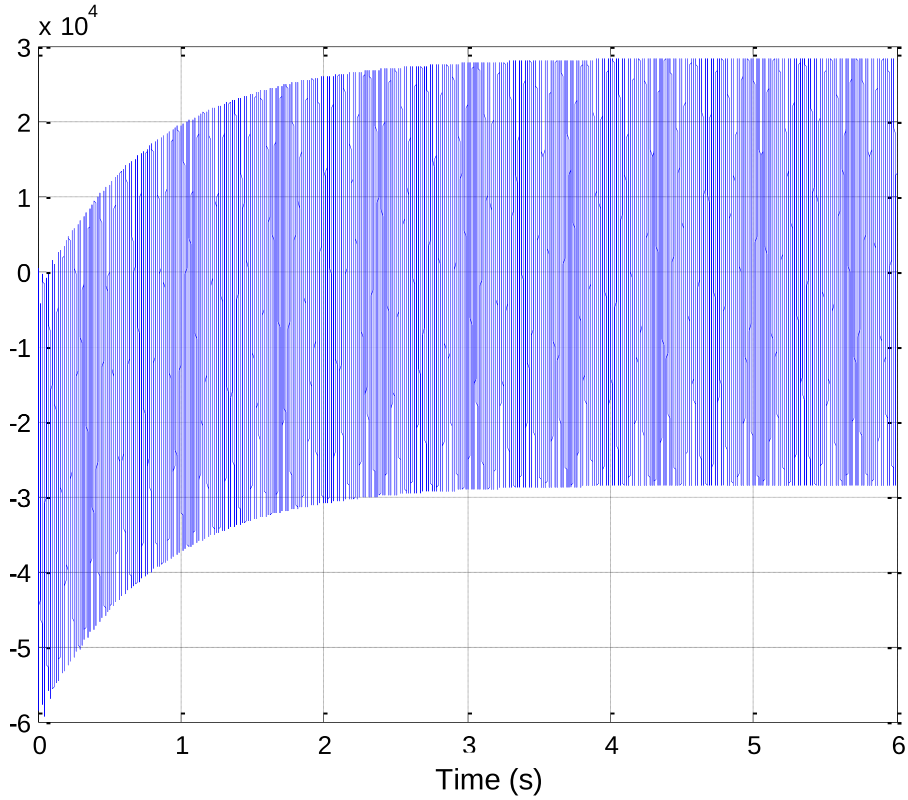

Figure 31 - Difference Between Upper and Lower Arm Energy (Joule)

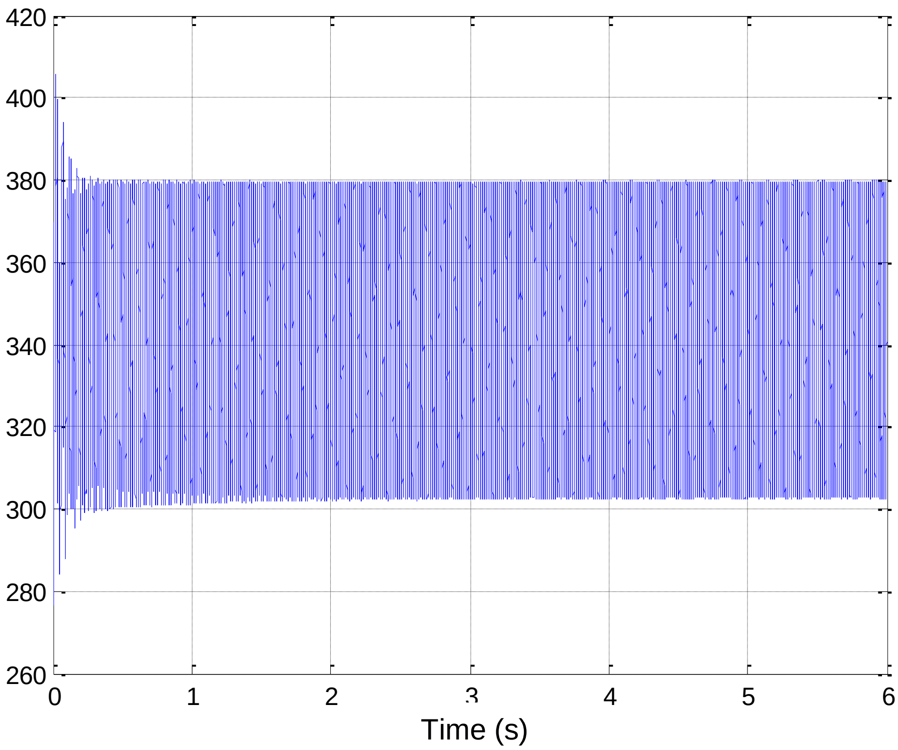

Figure 32 - Differential Current (A) in Steady State Conditions

In Fig. 32 differential current behavior is shown: continuous component increased proportionally to output current and line voltage, in order to balance output power increase. The alternate component remains limited and guarantees stability in upper and lower arm voltage. It is possible to notice the DC component, around 340 A, to balance output power and the AC component to balance Upper and Lower voltages.
Fig. 33 instead shows upper and lower arm voltages: as deepened in previous section, oscillations of these voltages are related to capacitors designed for the converter. In order to reduce the ripple it would be necessary to increase the capacitor in each sub-module: however, with the actual design and control tuning, voltage ripple is less than 1%.

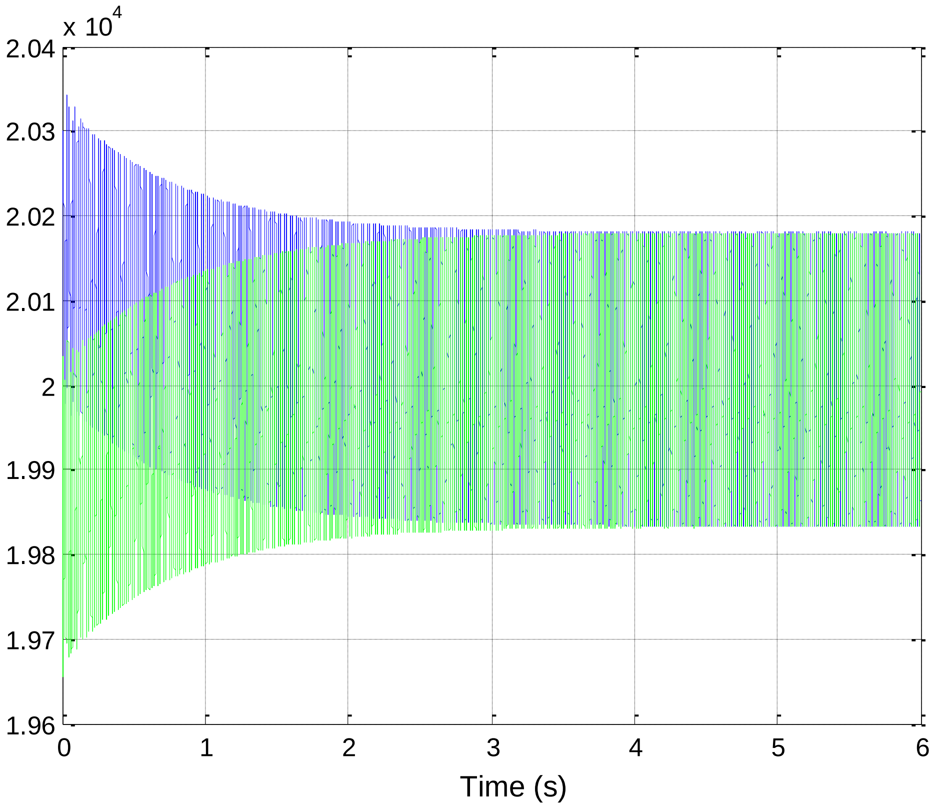

Figure 33 – Upper (Blue) and Lower (Green) Arm Voltages (V) in Steady State Conditions

The second simulation aims to test dynamic response of the system, in terms of step variation of the overall energy stored in the converter. As in previous models, this kind of simulation is not representative of a particular operating condition: it is however the best way to test control stability and performances of the total energy loop.
Even with a 50% change of the overall energy reference, the loop response respects all requirements: rising time is around *500 ms* and there is no overshoot or relevant oscillations around the new steady state condition, as represented in Fig. 34.

The influence of the overall energy loop on the balancing control loop is almost negligible, due to the frequency decoupling performed with control loops, and can be seen in Fig. 35.

From Fig. 36, it can be noted that differential current waveform respects all expectations: there is a short transient between initial and final steady state conditions in order to accomplish the overall energy reference change

The same dynamic response can be seen in upper and lower arm voltages as represented in Fig. 37.

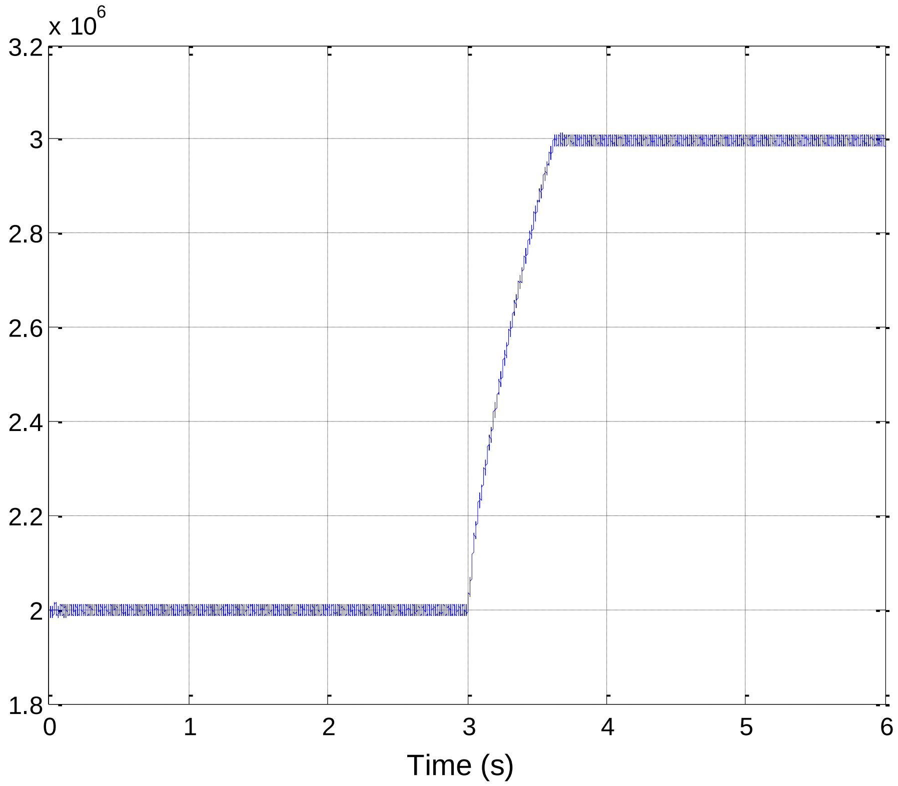

Figure 34 - Overall Energy (Joule) Step Response with a 50% Change of the Overall Energy Reference

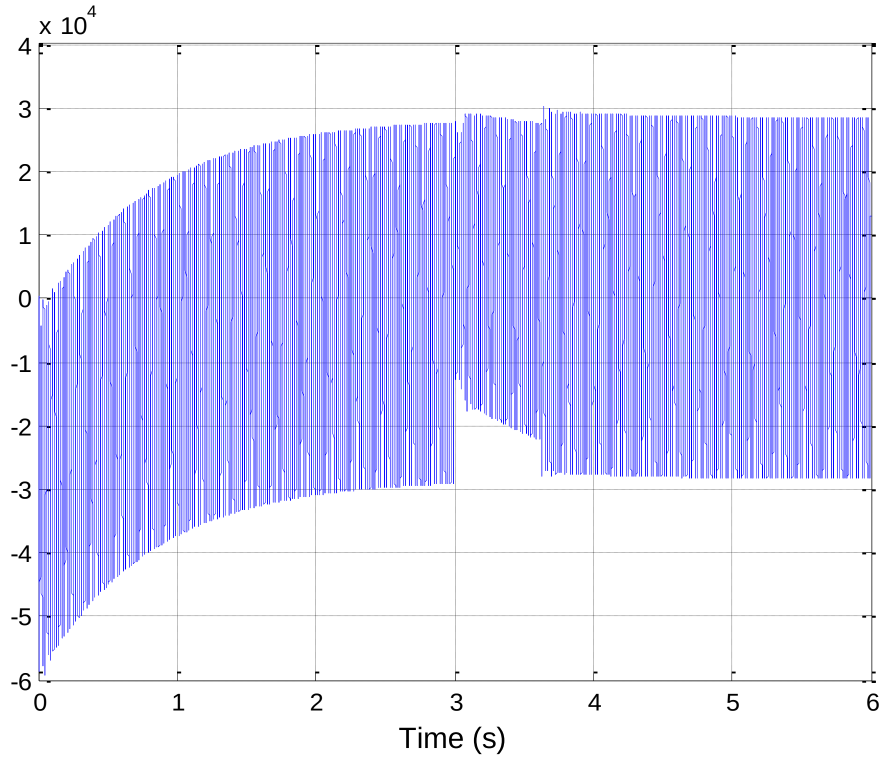

Figure 35 - Difference Between Upper and Lower Arm Energy (Joule) with a 50% Change of the Overall Energy Reference

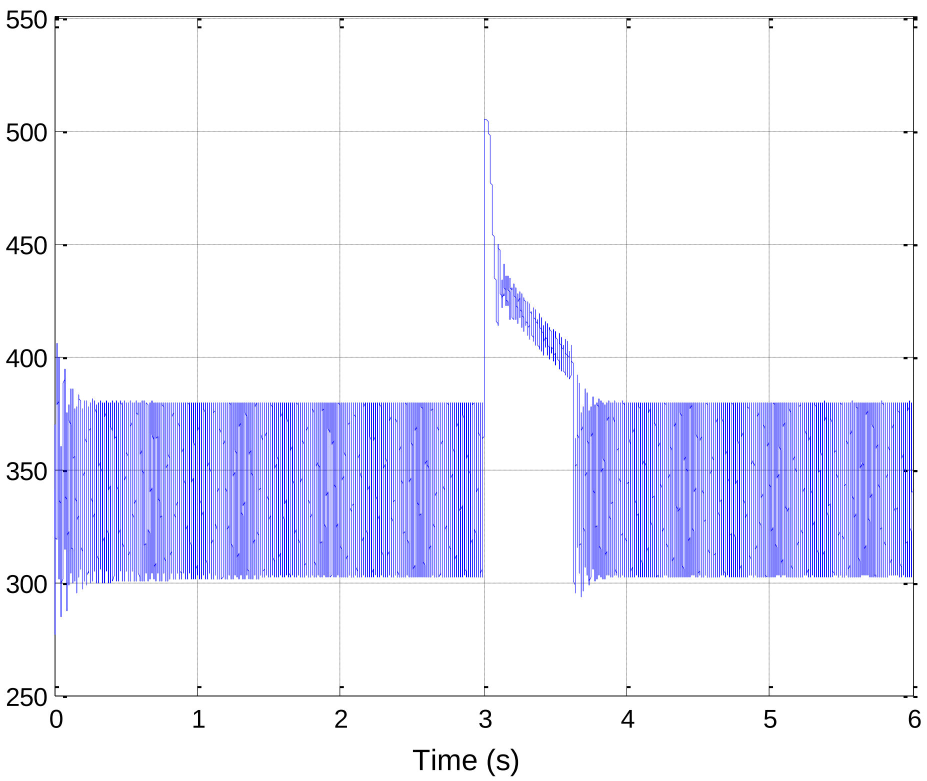

Figure 36 - Differential Current (A) Behavior with a 50% Change of the Overall Energy

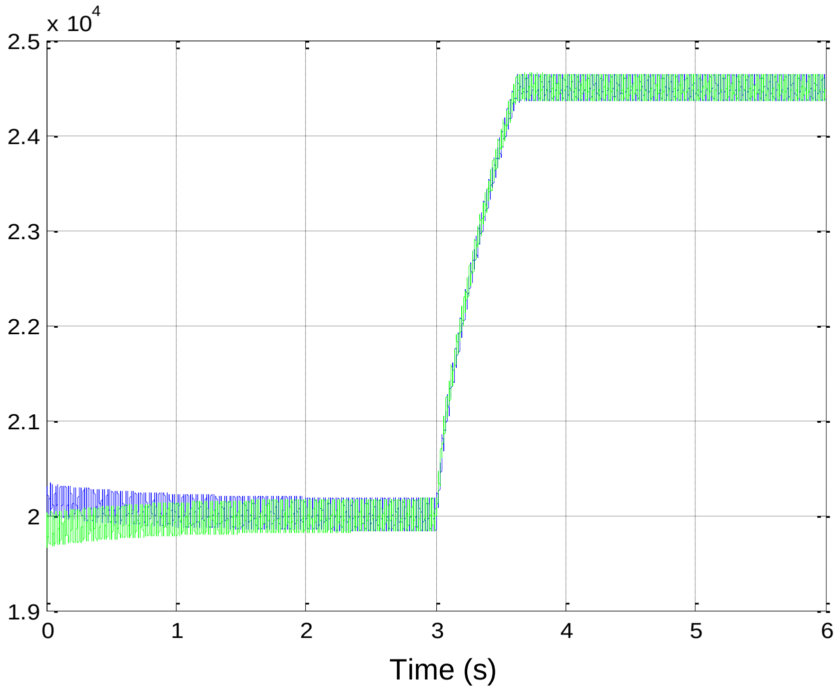

Figure 37 - Upper (Blue) and Lower (Green) Arm Voltages (V) with a 50% Change of the Overall Energy

4.5.3 - Simulation Results: Sub-Modules Failure Mode

In order to properly test also the balancing loop and to verify the coupling with overall energy loop further simulations are necessary: the initial condition of capacitors is set so that the system starts from an unbalanced condition. Thus, it will be possible to understand if the decoupling is possible in both directions of interaction: previous simulations showed that overall energy loop slightly influences balancing loop, but it is not possible to conclude the same for the opposite coupling.
This initial unbalance condition is related to a fault condition, where a certain number of broken sub-modules are bypassed: in order to remain in a fail-safe region, the control has to be fast and reliable, reaching the steady state condition without overshoots or oscillations.
Fig. 38 shows the overall energy behavior: starting from an unbalanced initial condition, the interaction between balancing loop and overall energy loop is not negligible.

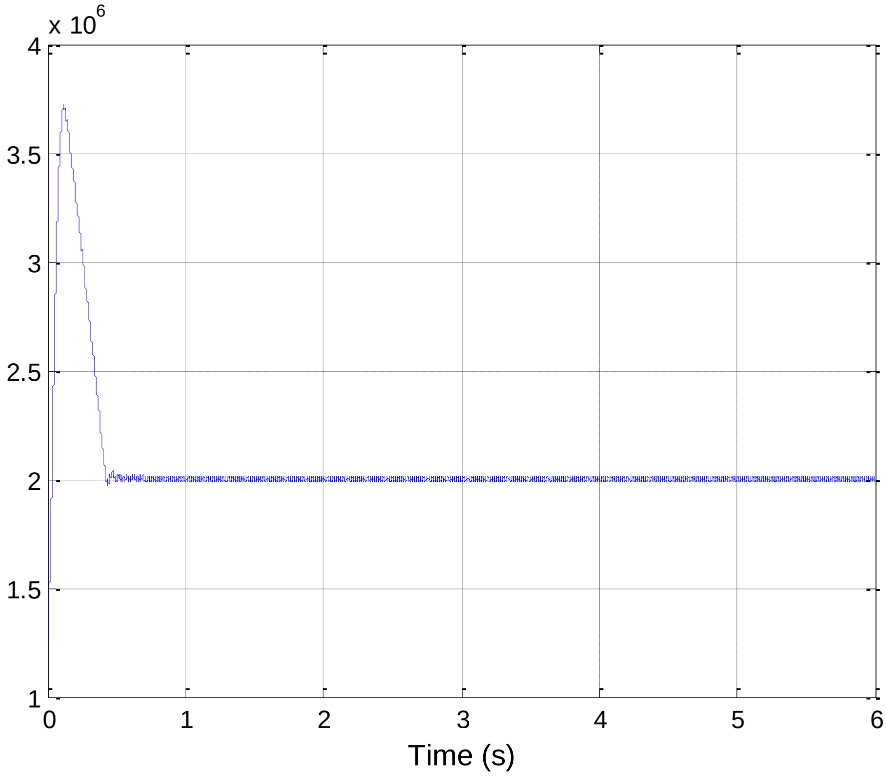

Figure 38 - Overall Energy (Joule): Response to Unbalanced Initial Conditions

The balancing loop acts slowly and takes a longer transient to set to zero the error, as can be noted in Fig. 39. The overall energy loop instead acts immediately to reach the steady-state reference value. As a consequence, the unbalanced initial condition leads to dangerous operation due to an important overshoot of the overall energy stored in capacitors, as clearly emphasized in Fig. 38.

The differential current flowing through the leg is the same for both upper and lower sub-modules: even if only one of the arms needs to be charged, the differential current will charge both of them, leading to a condition where the overall energy of the system overshoots greatly the reference value. This can be clearly understood analyzing the upper and lower arm voltage waveforms, shown in Fig. 40. It is possible to notice the overshoot of booth voltages, due to the same charging current.

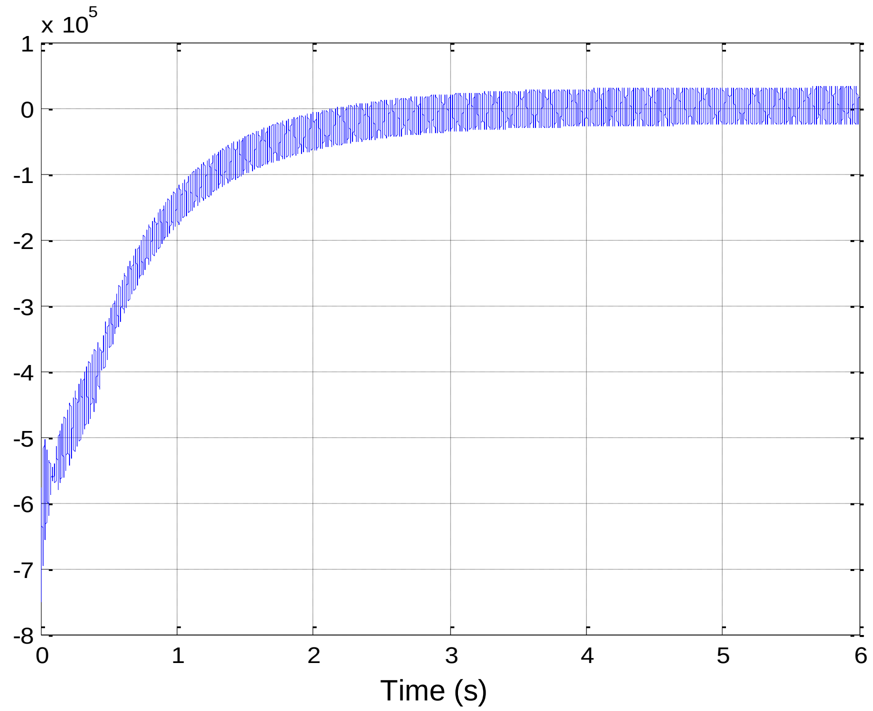

Figure 39 - Difference between Upper and Lower Arm Energy (Joule): System Response to Unbalanced Initial Conditions

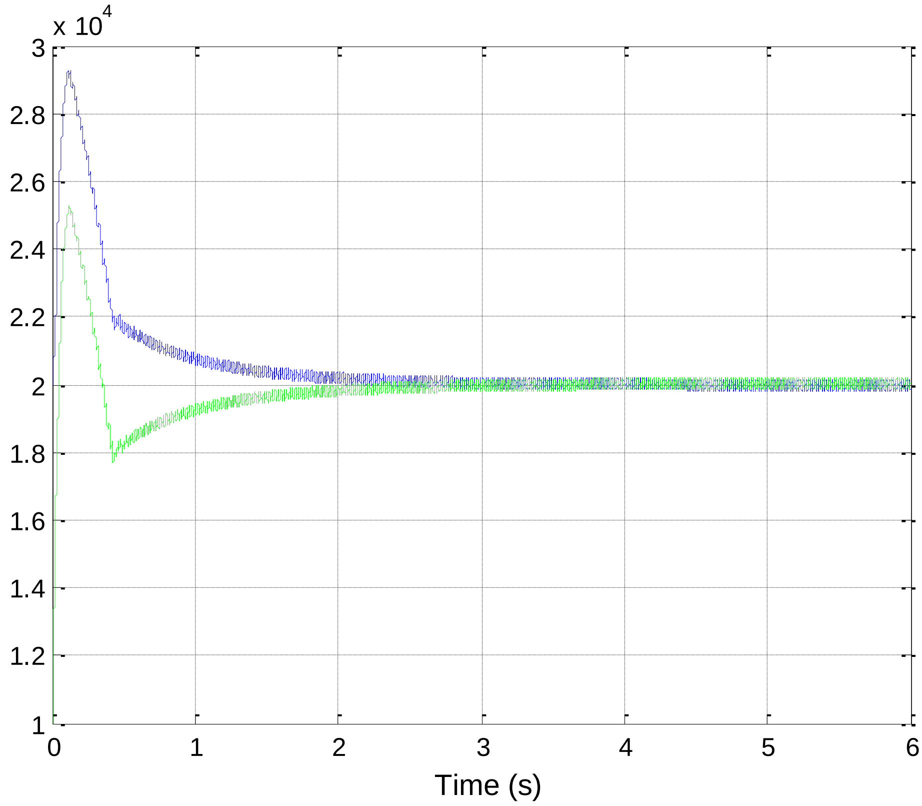

Figure 40 - Upper (Blue) and Lower (Green) Arm Voltages (V): System Response to Unbalanced Initial Conditions

The balancing loop acts as a disturbance for the overall energy loop, trying to reduce the unbalance with the same charging current and thus slowing down the dynamic response of voltages.
In order to reach the overall energy reference, control loop requires a high value of differential current, which instantaneously charges both upper and lower capacitors.
The problem is mainly caused by the fast response of the overall energy loop: the differential current required, in order to set to zero the error, charges both upper and lower arm sub-modules, leading to a non-acceptable overshoot.
Thus an improvement in the control strategy is required, taking into account that the differential current will charge anyway both upper and lower sub-modules.
In the event that one could ignore output variables behavior during the transient, it would be easy to eliminate the overshoot: the already charged arm would be bypassed, eluding the problem shown in previous simulations. But, as the tracking of output variable references is imposed, no significant improvement can be obtained from “low level” control.
Thus, the best solution is to work directly on the differential current: this approach will permit to guarantee output variables to follow reference (with just a brief transient) and reduce significantly overshoot in the energy response.
It is important to note that a significant overshoot reduction cannot be achieved retuning the parameters of regulators; this because the small capacitors used in sub-modules have a charging dynamic too fast for preventing completely overshoots by acting on the converter regulators .
In this thesis, parameters will not be changed, but instead an improved control scheme will be investigated and proposed. In order to prevent energy and voltage overshoots, differential current is monitored and controlled. As it is not possible to directly control this current, thus a feed-back-like structure is realized on the differential voltage loop that influences overall energy loop.
If differential current overcomes a safe range, a proportional action acts in order to decrease the differential voltage contribution and thus limit differential current. In Fig. 41 the scheme representing the principle of operation is shown. Violet blocks are used to compare differential current with an equivalent saturated current (saturation is imposed to remain in a safe range of operation) and a proportional controller is then imposed to the “error”.
Figs. 42 and 44 show the improvement of energy and arm voltages behavior: the differential current control reduces arm voltages overshoots, and thus overall energy overshoot. Actually, uncharged sub-modules reach voltage reference smoothly, without overshoots: the already charged arm has however a small overshoot, due to charging current. The behavior of the converter is now acceptable, and the overall energy overshoot is less than 10%. Balancing of energy behavior remains almost the same, compared to previous simulations and it is shown in Fig. 43.

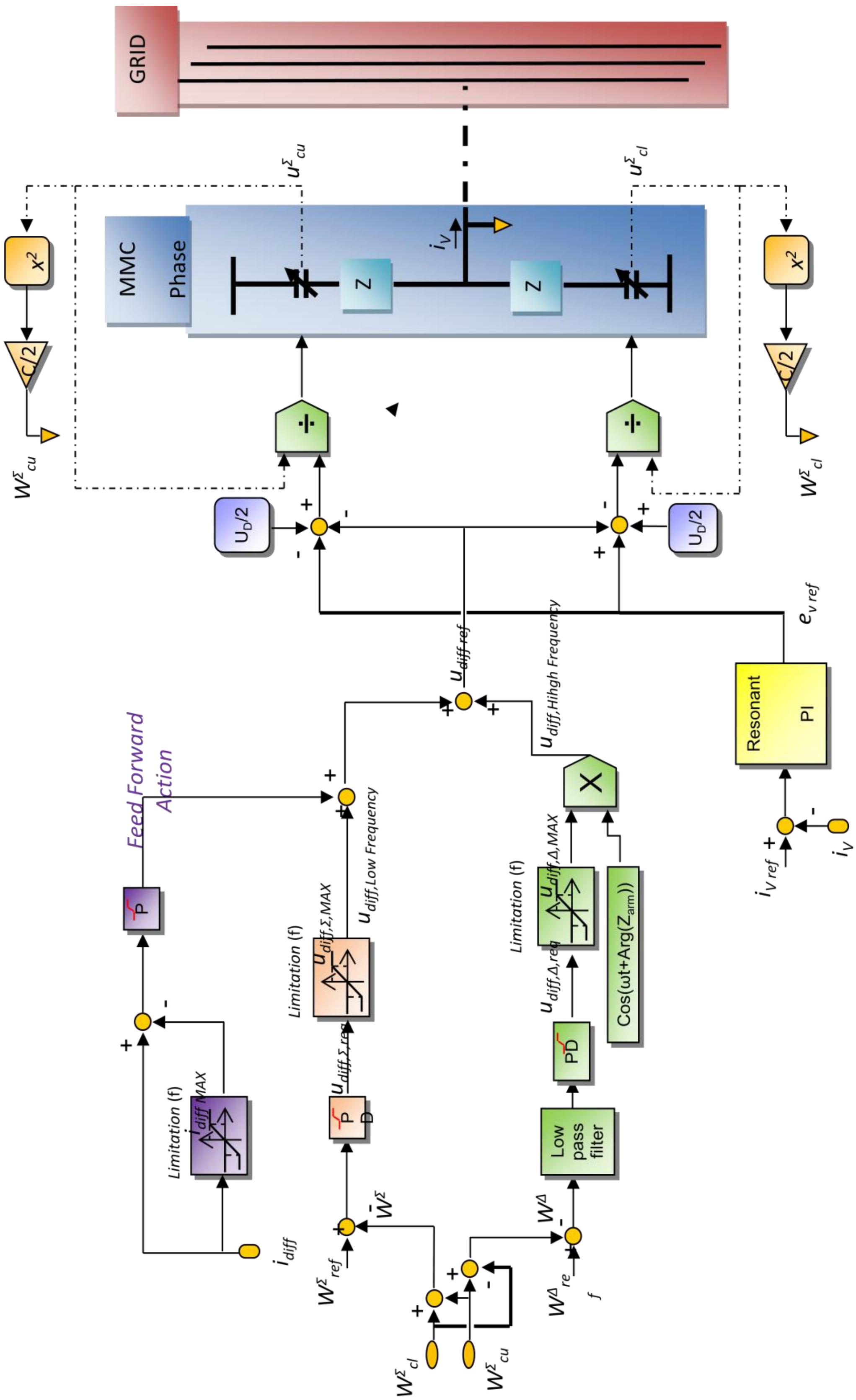

Figure 41 - Improved Control Strategy

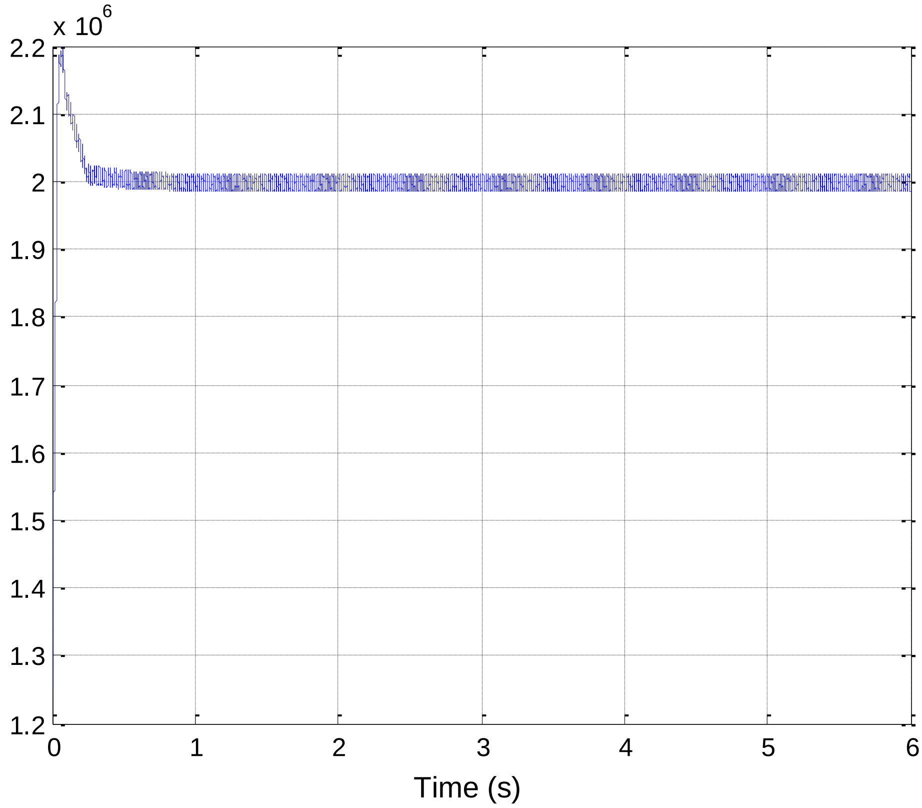

Figure 42 - Overall Energy (Joule): System response from an unbalanced initial condition with the new regulator

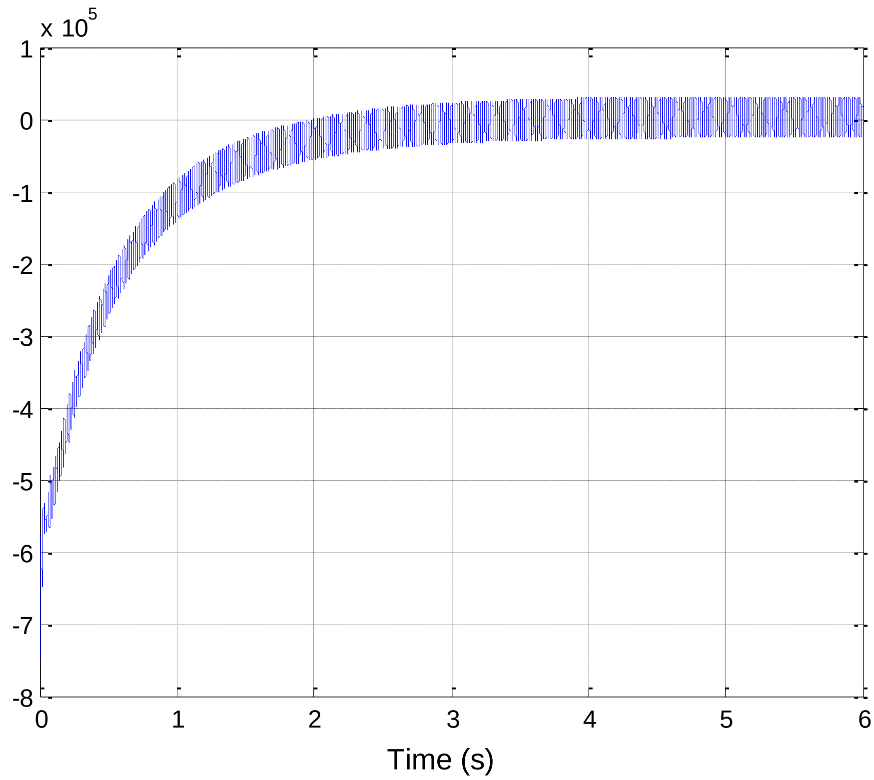

Figure 43 - Difference between Upper and Lower Arm Energy (Joule): System response from an unbalanced initial condition with new regulator

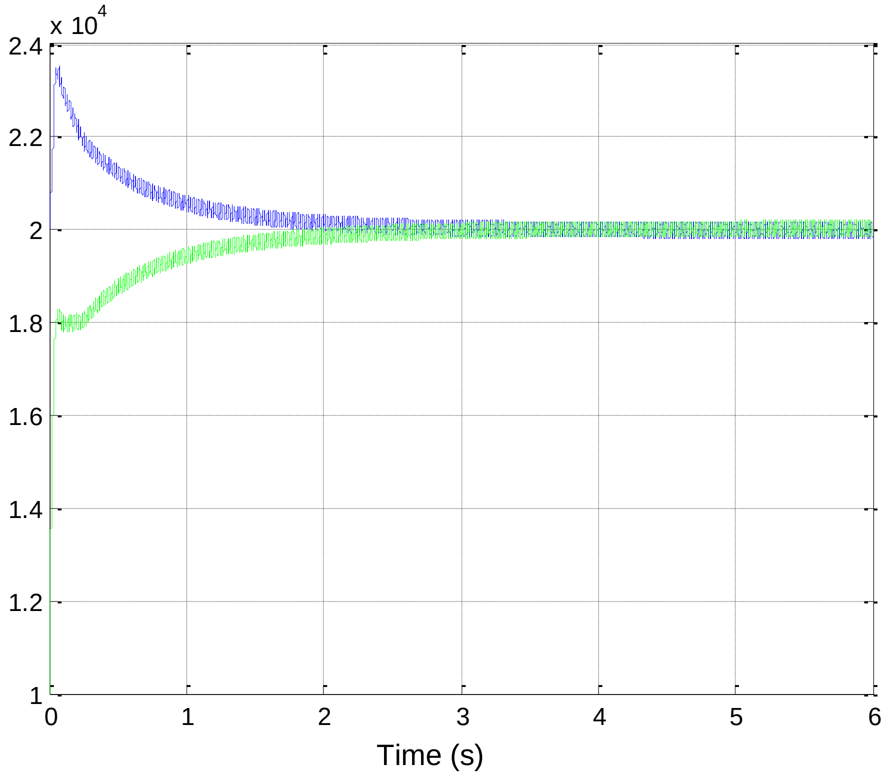

Figure 44 - Upper (Blue) and Lower (Green) Arm Voltages (V): System response from an unbalanced initial condition with the new regulator

4.5.4 - Simulation Results: LVRT

Last simulations shown in this thesis are related to Low Voltage Ride Through issue: in order to simulate this operating condition, grid voltage is set to zero for *200 ms* as represented in Fig. 45.

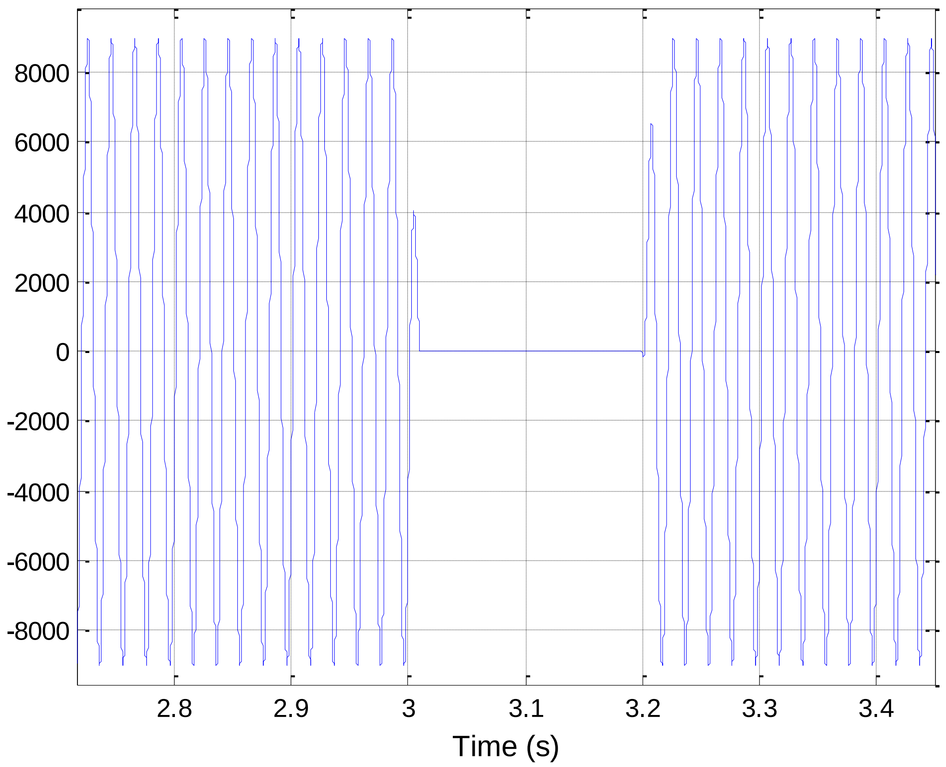

Figure 45 – Grid Voltage (V) during LVRT

The aim of this simulation is to see the energy behavior of the system; internal transient and current ripples need a more precise and focused modeling approach, but it is not in the scope of this thesis. What the simulation is supposed to proof is the reliability and safety of energy control system in faulty operating conditions.

It is plausible to expect a transient before the system reaches a new “fail” steady-state: after this condition, a new transient will lead the system back to the healthy operating conditions.

Actually, the system behavior fulfills expectations: as shown in Fig. 46, the overall energy is stable and has a small transient, leading to a steady-state condition.

Balancing control too, is able to maintain upper and lower arm voltages to the same desired value, as illustrated in Fig. 47.

Fig. 48 and 49 show the waveforms of capacitor voltages and differential current, respectively. The transient during LVRT is coherent with what expected. Differential current mean value is zero during the fault as the output power drops to zero. The alternate component instead remains almost unchanged, in order to maintain the balance between upper and lower arm voltages.

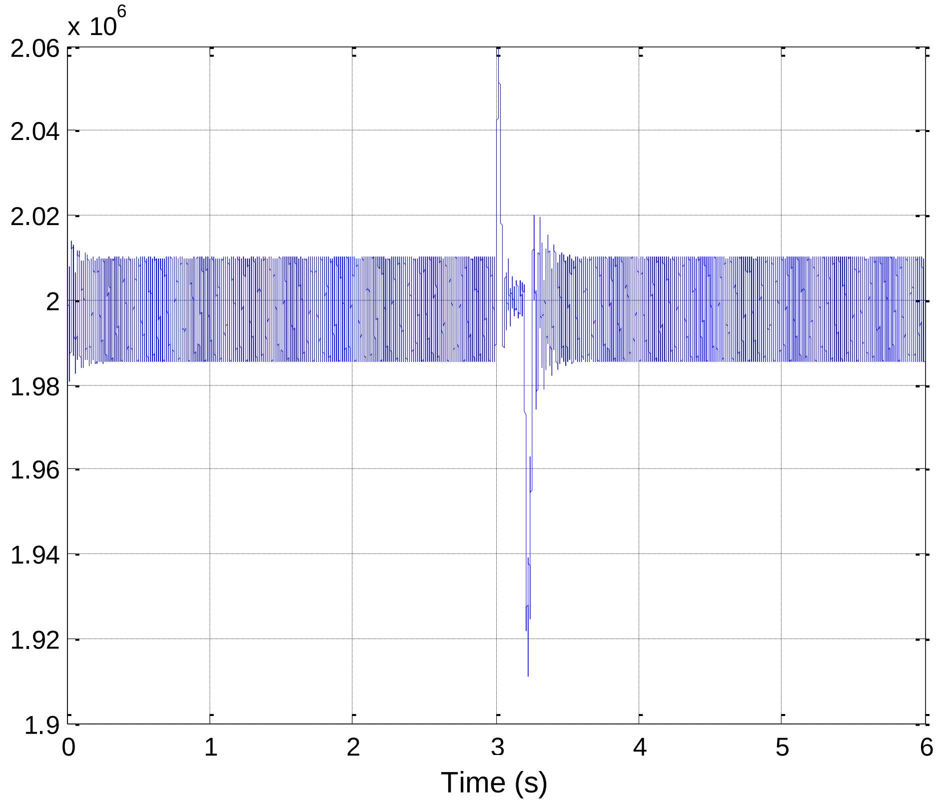

Figure 46 - Overall Energy (Joule): Behavior in LVRT condition

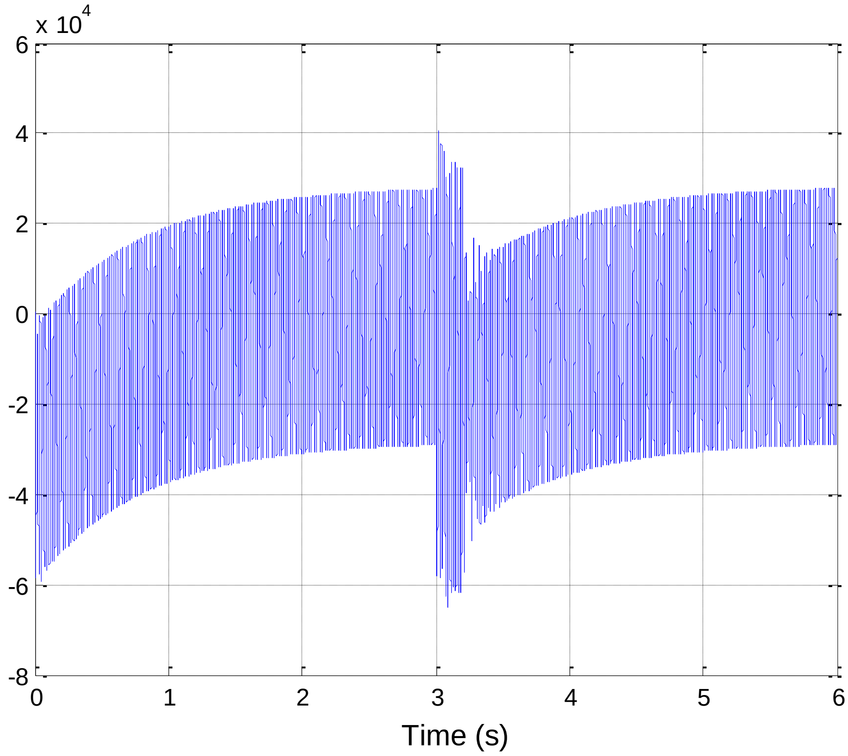

Figure 47 - Difference between Upper and Lower Arm Energy (Joule): Behavior in LVRT condition

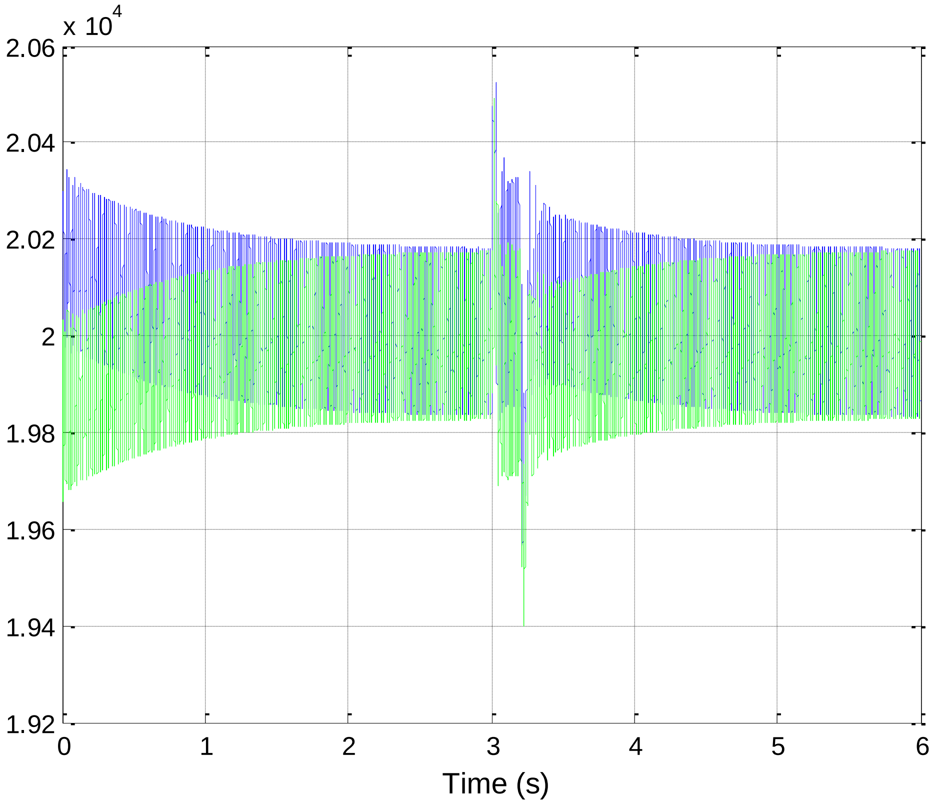

Figure 48 – Upper (Blue) and Lower (Green) Arm Voltages (V): Behavior in LVRT condition

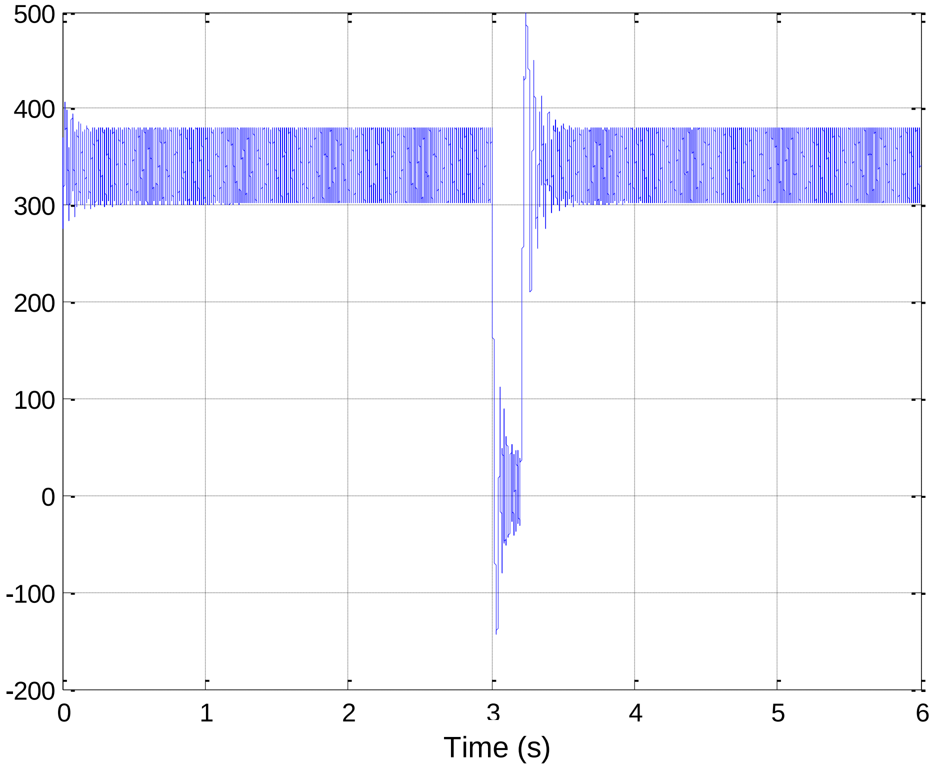

Figure 49 - Differential Current (A): Behavior in LVRT condition

Chapter V

5.1 – Motivation for a new modelling approach

From results obtained and showed in previous chapter, it possible to conclude that linear control behaves properly in steady state condition and in certain dynamic operation condition.

However, as underlined in Section 3.3, it is really hard to investigate advanced and robust control strategy, due to high non linearity in model equations.

Even if the linear control strategy gives a satisfying response, parameters changing, failure modes, fast dynamic requirements scenarios may introduce problems in the stability of the system: thus, these possibilities call for a deepening in different control approaches (for instance adaptive, robust, feedback linearization, optimal control etc).

In order to facilitate these studies, a new model approach here is proposed: the aim of this modelling approach is to obtain “more linear” equations: even if it is not possible to derive a completely linear model, it is desirable to apply advance control techniques to a simpler set of equations.

5.2 – Modelling Principles and Equations

A new simplified schematic of the MMC leg is proposed and shown in Fig: 50: grid is not [illegible]ed because not strictly necessary in this analysis, but must be introduced to build a simulation model.

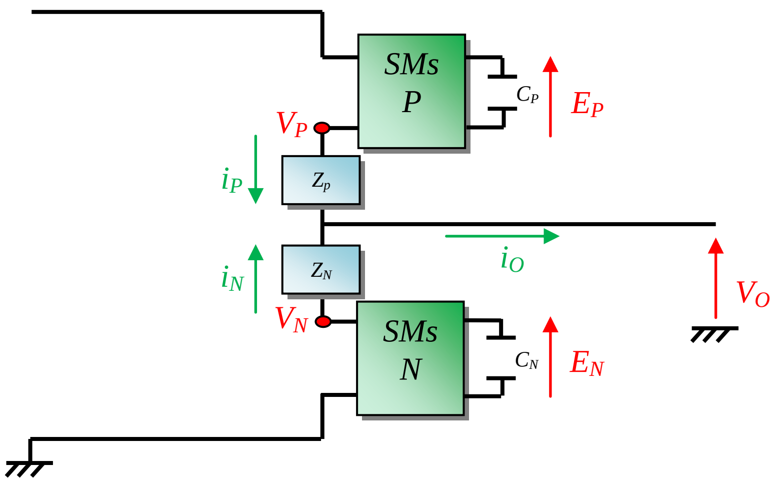

Figure 50 - New Simplified MMC Leg Model

With reference to Fig 50, it is possible to write voltage loop and current equations following Kirchhoff's laws.

$$V_P - V_O = L_P \frac{di_P}{dt} + R_P i_P \tag{46}$$

$$V_N - V_O = L_N \frac{di_N}{dt} + R_N i_N \tag{47}$$

$$i_O = i_P + i_N \tag{48}$$

Defining S_p and S_n as modulation indexes, respectively of upper and lower arms, it is possible to write:

$$E_{DC} - V_P = S_P E_P \tag{49}$$

$$V_N = S_N E_N \tag{50}$$

It is also possible to define dynamic equations for equivalent capacitors voltages, depending on modulation indexes:

$$C_P \frac{dE_P}{dt} = S_P i_P \tag{51}$$

$$C_N \frac{dE_N}{dt} = -S_N i_N \tag{52}$$

It is possible to assume that output current reference is assigned: the problem of controlling this current has a consequence in arm currents control.
These arm currents are supposed to maintain the overall energy to a desired value, to balance the difference between upper and lower arm energy and to guarantee output current to follow assigned set-point.
Thus, it is possible to write equations (53) and (54), in which the differential current is introduced:

$$i_{P\,ref} + i_{N\,ref} = i_{O\,ref} \tag{53}$$

$$i_{D\,ref} = i_{P\,ref} - i_{N\,ref} \tag{54}$$

From (53) and (54), it is possible to calculate upper and lower arm current references:

$$i_{P\,ref} = \frac{i_{O\,ref} + i_{D\,ref}}{2} \tag{55}$$

$$i_{N\,ref} = \frac{i_{O\,ref} - i_{D\,ref}}{2} \tag{56}$$

The problem can be easily solved if differential current reference is assigned: as mentioned before, this quantity has to be determined in order to maintain sub-module capacitors charged and balanced.
Using equations (55) and (56) it is possible to calculate the arm current references, then it is possible to create the current control loops as represented in Fig. 51.

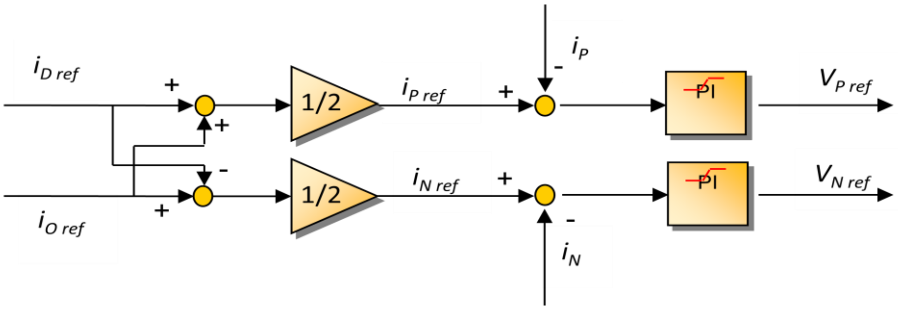

Figure 51 - Currents Control Loops

From equations (49) and (50) it is then possible to calculate modulation indexes, whose expressions are given in (57) and (58):

$$S_{P\,ref} = \frac{E_{DC} - V_{P\,ref}}{E_P} \tag{57}$$

$$S_{N\,ref} = \frac{V_{N\,ref}}{E_N} \tag{58}$$

In order to find differential current reference, it is necessary to write and analyze energy equations of MMC leg: instead of writing upper and lower energy equations, total energy and unbalance energy equations are suggested.
Let's consider W_T and W_D as total energy and difference energy between upper and lower arms, respectively:

$$W_T = \frac{1}{2}C_P E_P^2 + \frac{1}{2}C_N E_N^2 + \frac{1}{2}L_P i_P^2 + \frac{1}{2}L_N i_N^2 + \frac{1}{2}R_P i_P^2 + \frac{1}{2}R_N i_N^2 \tag{59}$$

$$W_D = \frac{1}{2}C_P E_P^2 - \frac{1}{2}C_N E_N^2 + \frac{1}{2}L_P i_P^2 - \frac{1}{2}L_N i_N^2 + \frac{1}{2}R_P i_P^2 - \frac{1}{2}R_N i_N^2 \qquad (60)$$

Introducing capacitor voltages and currents references, then equations (61) and (62) are obtained:

$$W_{T\,ref} = \frac{1}{2}C_P E_{P\,ref}^2 + \frac{1}{2}C_N E_{N\,ref}^2 + \frac{1}{2}L_P i_{P\,ref}^2 + \frac{1}{2}L_N i_{N\,ref}^2 + \frac{1}{2}R_P i_{P\,ref}^2 + \frac{1}{2}R_N i_{N\,ref}^2 \qquad (61)$$

$$W_{D\,ref} = \frac{1}{2}C_P E_{P\,ref}^2 - \frac{1}{2}C_N E_{N\,ref}^2 + \frac{1}{2}L_P i_{P\,ref}^2 - \frac{1}{2}L_N i_{N\,ref}^2 + \frac{1}{2}R_P i_{P\,ref}^2 - \frac{1}{2}R_N i_{N\,ref}^2 \qquad (62)$$

It is possible to assume that voltage drop contribution created by currents on arm impedance is negligible in comparison with capacitors voltage contribution: in order to find a dynamic relationship between energy variations and variables available to control MMC, equations (63) and (64) are introduced.

$$\frac{dW_T}{dt} = (E_{DC} - V_O)i_P - V_O i_N \qquad (63)$$

$$\frac{dW_D}{dt} = (E_{DC} - V_O)i_P + V_O i_N \qquad (64)$$

It is necessary to point out differential current contribution: thus, substituting upper and lower arm currents with their reference expressions, i.e. equations (55) and (56), yields to

$$\frac{dW_T}{dt} = (E_{DC} - V_O)\frac{i_O + i_D}{2} - V_O\frac{i_O - i_D}{2} = \left(\frac{E_{DC}}{2} - V_O\right)i_O + \frac{E_{DC}}{2}i_D \qquad (65)$$

$$\frac{dW_D}{dt} = (E_{DC} - V_O)\frac{i_O + i_D}{2} + V_O\frac{i_O - i_D}{2} = \frac{E_{DC}}{2}i_O + \left(\frac{E_{DC}}{2} - V_O\right)i_D \qquad (66)$$

If output current and voltage are periodical functions, with period T_0 it is possible to integrate equations (65) and (66), leading to

$$\Delta W_T = \int_0^{T_0}\left(\frac{E_{DC}}{2} - V_O\right)i_O dt + \frac{E_{DC}}{2}\int_0^{T_0} i_D dt \qquad (67)$$

$$\Delta W_D = \frac{E_{DC}}{2}\int_0^{T_0} i_O dt + \int_0^{T_0}\left(\frac{E_{DC}}{2} - V_O\right) i_D dt \qquad (68)$$

These equations show clearly differential current contribution in system energy dynamic operation: total energy WT depends form differential current mean value, W_D instead depends form the alternate component of differential current having the same frequency as output voltage.

These considerations can be summarized with the following scheme, Fig. 52.

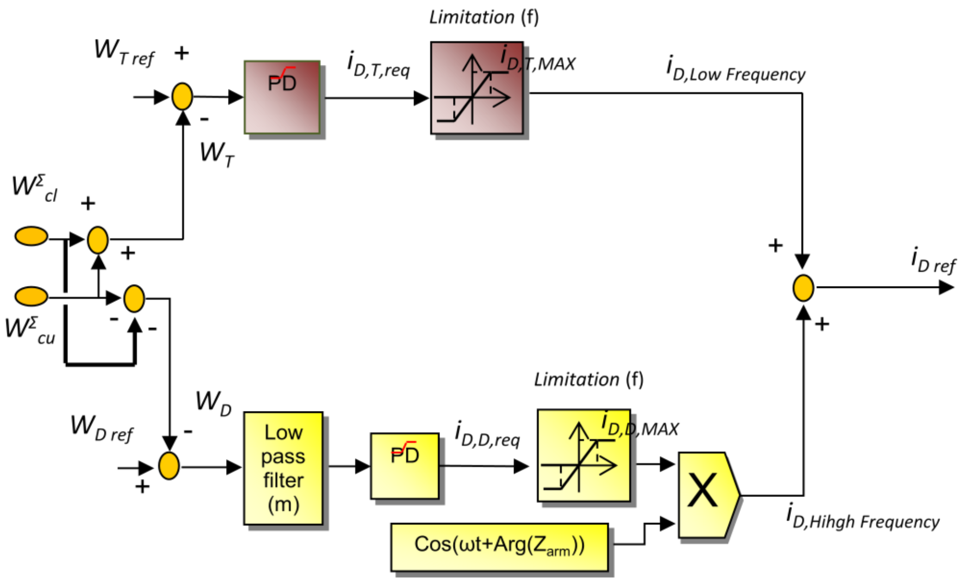

Figure 52 – Energy Control Scheme Diagram

5.3 – Control Proposal

In this Section, control scheme previously described is explained extensively.

Compared with the control approach of Chapter III, used for simulation results in Chapter IV, this new approach provides a cascade structure.

Two different loops are realized, an energy loop and a differential current loop: energy loop provides a differential current reference, which is tracked by the current control loop.

Energy loop is composed of overall energy control and balancing control.

Current loop is composed of upper current control and lower current control.

The complete control scheme is shown in Fig. 53.

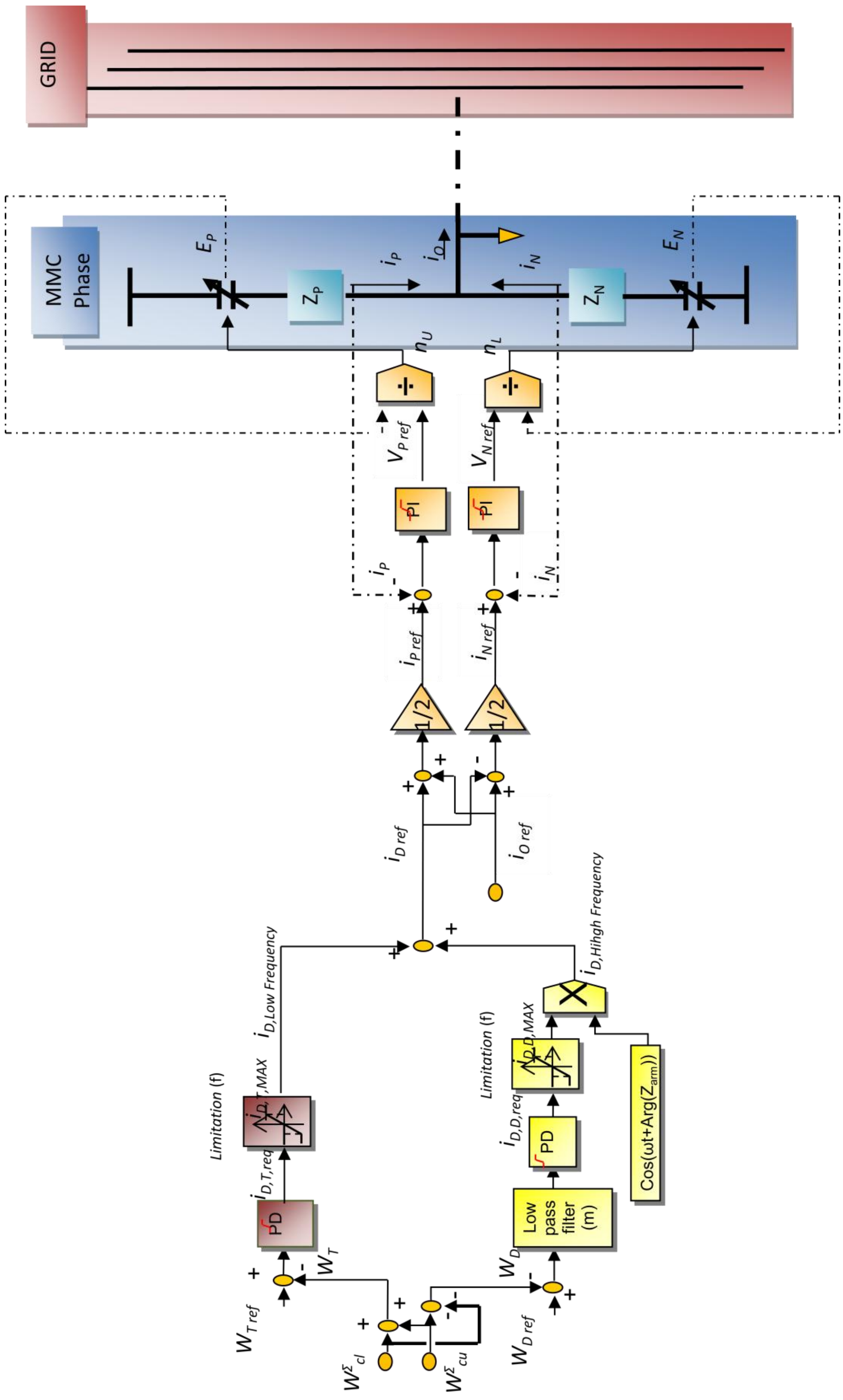

Figure 53 - Control Scheme for new Modeling Approach

Following equations (46) and (47), current control loop is pretty easy to be tuned: actually, between upper and lower arm voltages and arm currents only an *R-L* low pass filter is present. Then, through equations (49) and (50), modulation indexes, real system input, can be calculated.

Once control loop is tuned, it is possible to work on energy loop: using equations (65) and (66), it is possible to control total energy and balancing dynamics. Thus, an integrator is not necessary to set to zero total energy error and balancing error (i.e. an integrator is intrinsically present in the system).

Control suggested and shown in Fig. 53 includes PD controller: this control structure is again based on a frequency decoupling, where balancing loop is tuned to be slower than total energy loop.

Simulation parameters chosen are the same used in the Mega-Watt system discussed in Section 4.5.

In Figs. 54, 55 and 56, the simulation of a steady state condition is shown: the initial transient is due to equation structure. A differential current derivative equation is not present in the model, thus it is not possible to impose the initial condition.

It is however possible to see that after *2 s* a steady state condition is reached without overshoot or oscillation.

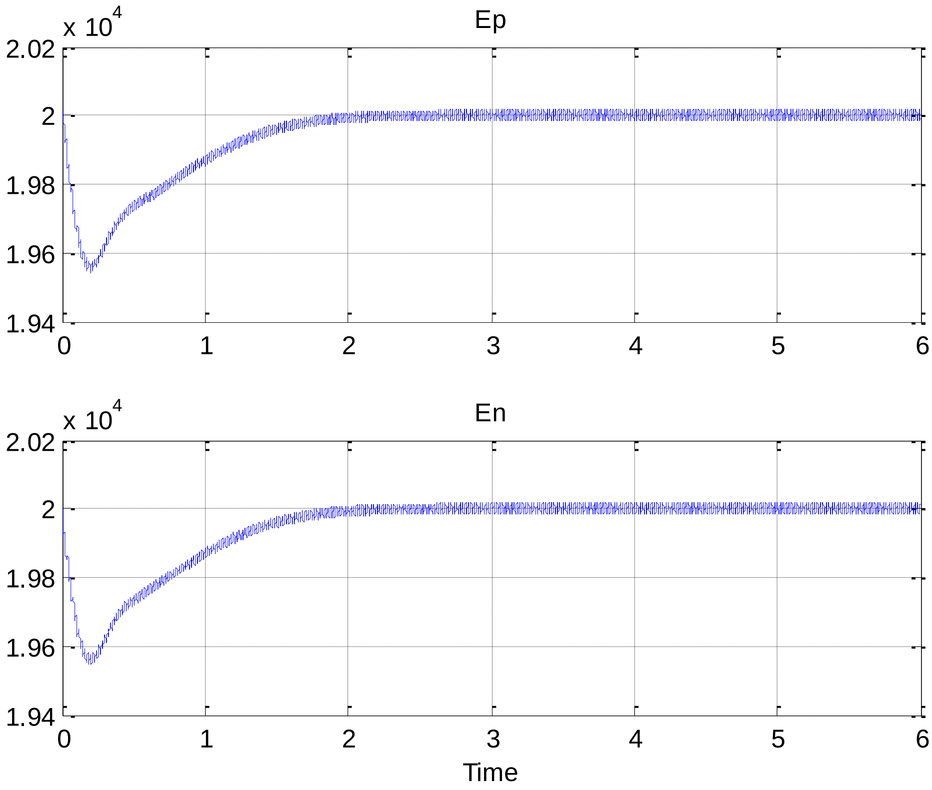

Figure 54 - Upper and Lower Arm Capacitor Voltages

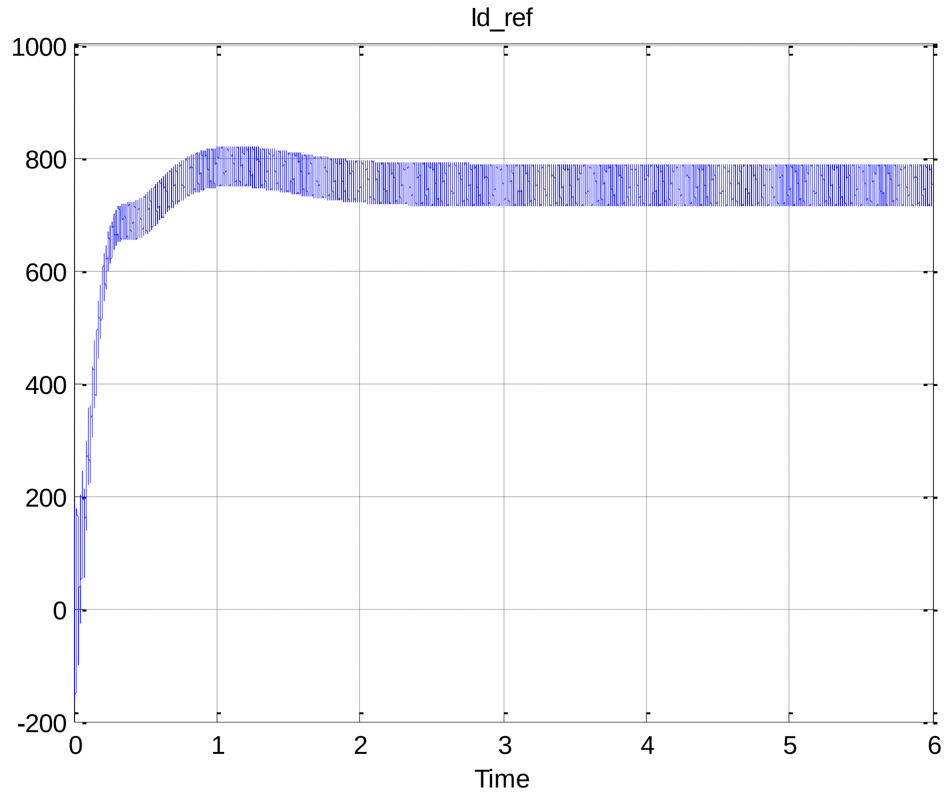

Figure 55 - Differential Current Transient (A)

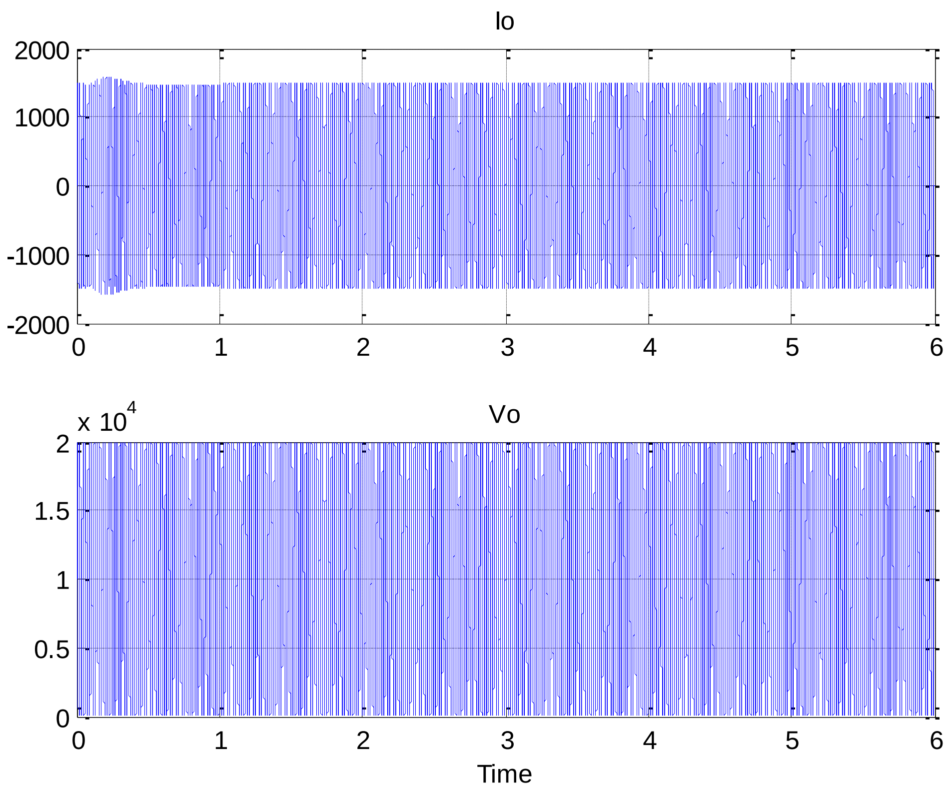

Figure 56 - Output Current (A) and Output Voltage (V)

Further simulations, concerning dynamic behaviour of the system, will be carried out in the near future: however, it was considered important to show a simple simulation introducing the validity of the approach.
A comparison with model proposed in [8] (that has been used in the beginning of this thesis to deepen system operation and control strategies) will also be developed: as an introduction, next Section will briefly compare the equations of the two models in order to propose future control possibilities.

5.4 – Future Works

Besides to basic control strategy described in previous paragraph, new modeling approach gives a set of equations which are easier to be used in order to deepen advanced control strategies.
It is possible to compare energy equations between the new proposed model and the model described in [8]:

$$\frac{dW_C^{\Sigma}}{dt} = (u_D - 2u_{diff})i_{diff} - e_V i_V \tag{34}$$

$$\frac{dW_C^{\Delta}}{dt} = \left(\frac{u_D}{2} - u_{diff}\right) i_V - 2e_V i_{diff} \tag{35}$$

$$\frac{dW_T}{dt} = \left(\frac{E_{DC}}{2} - V_O\right) i_O + \frac{E_{DC}}{2} i_D \tag{65}$$

$$\frac{dW_D}{dt} = \frac{E_{DC}}{2} i_O + \left(\frac{E_{DC}}{2} - V_O\right) i_D \tag{66}$$

Neglecting notation differences, the high non-linearity of equations (34) and (35) is smoothed considerably in equations (65) and (66).
Total energy in equations (34) is controlled through differential current, which is a “square” non-linear input for the system (see Section3.3): in equation (65) instead, the input is linear because the differential current is multiplying the DC voltage, which can be considered constant.
A similar consideration may be done about balancing equations: equation (35) is highly non-linear for input variables (differential voltage and differential current), instead equation (66) has a component of the input which is still linear and can be used to implement advanced control strategies.
Equations (34) and (35) give few chances to develop advanced control techniques, due to their intrinsic non-linear structure.

Equations (65) and (66) instead, make it easier to define advanced control strategies based on model inversion, feed-forward actions, and feed-back linearization.

All these possibilities will be investigated in near future and their functionality and performances will be compared with standard linear controllers already implemented and discussed in this work.

Chapter VI – Conclusions

The aim of this project was the analysis of a Modular Multilevel Converter (MMC) for wind farm applications and the development of a control scheme to monitor the energy behavior.

The analysis was based on the use of a simplified circuit, constituted by a single leg of the converter, where all the modules in each arm were represented by a single variable voltage source. The circuit model was derived as a system of differential equations, used for analyzing both the steady state and dynamic behavior of the MMC, from voltages and thus energy point of view.

Preliminary analysis was carried out following the modeling approach proposed in [8]. Using this model, the system behavior has been studied and a possible energy control scheme has been developed. The numerical simulations have shown that the system is operating correctly under steady-state and transient operating conditions, except for initial conditions with unbalanced capacitor voltages. To reduce the large voltage overshoots due to this unbalanced initial condition, an improved control scheme has been developed.

In Chapter V, a new modeling approach was proposed, aiming to define a set of equations more suitable for advanced control implementation.

With the new modeling approach a significant contribution to control issues will be possible: in the near future, a comparison between the new modeling approach and the one proposed in [8] will be investigated.

New control structures will also be developed, in order to accomplish all dynamic requirements required by the particular application, i.e. to comply with the new grid code standards.

REFERENCES

[1] J. Rodriguez, J. S. Lai, and F. Z. Peng, " Multilevel Inverters: a survey of topologies, controls, and applications. " IEEE Trans. Ind. Electronics, vol. 49, no. 4, pp. 724-738, August 2002.

[2] A. Lesnicar, and R. Marquardt, "An Innovative Modular Multilevel Converter Topology Suitable for a Wide Power Range", IEEE PowerTech Conference, Bologna, Italy, June 23-26, 2003.

[3] A. Lesnicar, and R. Marquardt, "A new modular voltage source inverter topology", EPE 2003, Toulouse, France, September 2-4, 2003.

[4] R. Marquardt, and A. Lesnicar, "New Concept for High Voltage - Modular Multilevel Converter", IEEE PESC 2004, Aachen, Germany, June 2004.

[5] M. Glinka and R. Marquardt, "A New AC/AC Multilevel Converter Family", IEEE Transactions on Industrial Electronics, vol. 52, no. 3, June 2005.

[6] B. Gemmel, J. Dorn, D. Retzmann, and D. Soerangr, "Prospects of multilevel VSC technologies for power transmission", in Conf. Rec. IEEE-TDCE 2008, pp. 1-6.

[7] M. Hagiwara, H. Akagi "PWM Control and Experiment of Modular Multilevel Converters", IEEE PESC 2008, Rhodes, Greece, June 2008.

[8] A. Antonopoulos, L. Angquist, and H.-P. Nee, "On dynamics and voltage control of the modular multilevel converter," European Power Electronics Conference (EPE), Barcelona, Spain, September 8-10, 2009.

[9] G.Bergna, M.Boyra, J.H.Vivas, "Evaluation and Proposal of MMC-HVDC Control Strategies under Transient and Steady State Conditions"

[10] P.Munch, S.Liu, M.Dommaschk "Modeling and Current Control of Modular Multilevel Converters Considering Actuator and Sensor Delays"

[11] M.Hagiwara, R.Maeda, H.Akagi, "Control and Analysis of the Modular Multilevel Cascade Converter Based on Double-Star Chopper-Cells (MMCC-DSCC)"

[12] W.Li, L.A.Regoire, J.Bèlanger OPAL-RT Technologies (CAN), "Control and Performance of a Modular Multilevel Converter System"

[13] S. Rohner, J. Weber and S. Bernet "Continuous Model of Modular Multilevel Converter with Experimental Verification", Dresden University of Technology